

Durham Research Online

Deposited in DRO:

15 December 2017

Version of attached file:

Accepted Version

Peer-review status of attached file:

Peer-reviewed

Citation for published item:

Rooney, A.D. and Austermann, J. and Smith, E.F. and Li, Y. and Selby, D. and Dehler, C.M. and Schmitz, M.D. and Karlstrom, K.E. and Macdonald, F.A. (2017) 'Coupled Re-Os and U-Pb geochronology of the Tonian Chuar Group, Grand Canyon.', *Geological Society of America bulletin.*, 130 (7-8). pp. 1085-1098.

Further information on publisher's website:

<https://doi.org/10.1130/B31768.1>

Publisher's copyright statement:

Additional information:

Use policy

The full-text may be used and/or reproduced, and given to third parties in any format or medium, without prior permission or charge, for personal research or study, educational, or not-for-profit purposes provided that:

- a full bibliographic reference is made to the original source
- a [link](#) is made to the metadata record in DRO
- the full-text is not changed in any way

The full-text must not be sold in any format or medium without the formal permission of the copyright holders.

Please consult the [full DRO policy](#) for further details.

Coupled Re-Os and U-Pb geochronology of the Tonian Chuar Group, Grand Canyon

Alan D. Rooney^{1*,2}, Jacqueline Austermann^{2,3}, Emily F. Smith^{2,4}, Yang Li^{1,5}, David Selby⁵, Carol M. Dehler⁶, Mark D. Schmitz⁷, Karl E. Karlstrom⁸, Francis A. Macdonald²

¹*Department of Geology and Geophysics, Yale University, New Haven, Connecticut, 06511, USA*

²*Department of Earth and Planetary Sciences, Harvard University, Cambridge, Massachusetts, 02138, USA*

³*Bullard Laboratories, Department of Earth Sciences, University of Cambridge, Cambridge, CB3 0EZ UK*

⁴*Department of Earth and Planetary Sciences, Johns Hopkins University, Baltimore, Maryland, 21218, USA*

⁵*Department of Earth Sciences, Durham University, Durham, DH1 3LE, UK*

⁶*Department of Geology, Utah State University, Logan, Utah, 84322, USA*

⁷*Department of Geosciences, Boise State University, Boise, Idaho, 83725, USA*

⁸*Department of Earth Sciences, University of New Mexico, Albuquerque, New Mexico, 87131, USA*

ABSTRACT

Well-preserved strata of the late Tonian Chuar Group exposed in the Grand Canyon host fossil evidence for the development of eukaryotic predation, the presence of unique biomarkers, and large changes in C, S and Mo isotope chemostratigraphy. Despite the importance of this critical succession, few radioisotopic age constraints are available to place these records into a global context. Here we couple high-precision U-Pb chemical abrasion isotope dilution thermal ionization mass spectrometry (CA-ID-TIMS) on zircon crystals with the rhenium-osmium (Re-Os) sedimentary and sulfide geochronometer to refine the temporal framework of this pivotal interval of Earth history. Zircons recovered from a tuff within the uppermost Walcott Member of the Kwagunt Formation yield a weighted mean ^{206}Pb - ^{238}U age of 729.0 ± 0.9 Ma (MSWD = 0.86) differing significantly from the previous air abrasion upper intercept age of 742 ± 6 Ma on zircons from this same horizon. Organic-rich carbonates from the Carbon Canyon Member of the Galeros Formation yield a Model 1 Re-Os age of 757.0 ± 6.8 Ma (MSWD = 0.47, $n = 8$), and an initial Os isotope [$^{187}\text{Os}/^{188}\text{Os}$, Osi] composition of 1.13 ± 0.02 . The radiogenic Osi value from this horizon suggests that the basin was restricted from the open ocean during deposition of the

Carbon Canyon Member, in agreement with sedimentological and stratigraphic data. The Re-Os geochronology of marcasite (FeS₂) nodules from the Awatubi Member of the Kwagunt Formation yield a Model 1 age of 751.0 ± 7.6 Ma (MSWD = 0.37, $n = 5$), with an *Osi* of 0.44 ± 0.01 . This Re-Os date is interpreted to constrain the growth of the marcasite nodules in the Awatubi Member. The formation of sulfides and the unradiogenic *Osi* value are consistent with an influx of sulfate-laden seawater to the basin during deposition of the Kwagunt Formation. Attempts to apply the Re-Os geochronometer to the Walcott and Tanner members of the Chuar Group failed to yield meaningful ages despite elevated Re enrichments (>20 ng/g). The Re-Os data from these units yield negative *Osi* values, which suggests disturbance to the Re-Os system. The low Os abundances (typically <100 pg/g) relative to the amount expected based on the elevated Re abundances suggests leaching of Os due to oxidative weathering on geologically recent timescales. Finally, the Carbon Canyon Member provides a useful case study for quantifying how input uncertainties in the Re-Os geochronometer propagate into the resulting age uncertainty, and we discuss the protocols that will yield the best improvement in age precision for future studies. U-Pb and Re-Os geochronology presented here illustrates the power of coupling these systems and the importance of recent improvements in both methods. Our analysis suggests that for our data the most efficient way of reducing uncertainties in the presented Re-Os dates is through improved precision of measured Os values.

INTRODUCTION

Tonian (1000-720 Ma) basins of western North America formed during the early stages of the breakup of the Rodinia supercontinent (Jefferson and Parish, 1989; Karlstrom et al., 2000; Li et al., 2013; Macdonald et al., 2013; Strauss et al., 2015; Smith et al., 2016). These sedimentary successions host evidence for the diversification and proliferation of eukaryotic organisms and large-magnitude perturbations to numerous biogeochemical proxy records, changes in oxygenation, (Narbonne et al., 1994; Halverson et al., 2005, 2010; Porter and Knoll, 2000; Porter et al., 2003; Knoll et al., 2006; Knoll, 2014; Planavsky et al., 2014; Strauss et al., 2014; Brocks et al., 2016; Dehler et al., 2017) and provide essential context for the lead-up to the pan-glacial conditions that characterized the Cryogenian Period (720-635 Ma; Macdonald et al., 2010; Rooney et al., 2014, 2015; Cox et al., 2016; Shields-Zhou et al., 2016). Further interpretations of the causality and tempo of Neoproterozoic environmental and biological

change have been restricted by a lack of radioisotopic age constraints and limited biostratigraphy. Organic-rich sedimentary strata and a tuff within the late Tonian Chuar Group exposed in the Grand Canyon (Fig. 1) offer an opportunity to refine the temporal framework of the Tonian using the Re-Os and U-Pb zircon geochronometers, and evaluate the consistency and reproducibility between these two techniques. Legacy U-Pb zircon data, carbon isotope data and diverse assemblages of vase-shaped microfossils (VSMs) within the Chuar Group (Karlstrom et al., 2000; Porter et al., 2003; Dehler et al., 2005) enable broad, first-order correlations with other extensional basins of western North America (Jefferson and Parrish, 1989; Macdonald et al., 2010, 2013; Mahon et al., 2014; Rooney et al., 2014, 2015; Strauss, et al., 2014; Dehler et al., 2017; Figs. 2 and 3). Here we present new Re-Os geochronology data from sedimentary rocks and marcasite (FeS₂) nodules of the Chuar Group together with a new high-precision U-Pb CA-ID-TIMS date on zircon grains from a volcanic tuff. These data provide improved constraints on the depositional history of this sedimentary archive and enhance correlations with other pre-Cryogenian strata globally. Additionally, we evaluate sources of uncertainty and the propagation of these uncertainties in the Re-Os system, and attempt to understand the main control of the final uncertainty in Re-Os ages, and make the statistical treatment of Re-Os geochronology data more transparent.

GEOLOGICAL SETTING

Exceptionally well-preserved sedimentary strata of the Tonian Chuar Group are exposed in a broad, doubly plunging syncline with spectacular outcrops found along several tributaries of the Colorado River in the eastern region of the Grand Canyon, AZ, USA (Fig. 1). Locally, the Chuar Group is unconformably overlain by the Cambrian Sixtymile and Tapeats formations and unconformably overlies the Mesoproterozoic Unkar Group (Fig. 2; Timmons et al., 2001). The Chuar Group is a ~1600-m-thick succession dominated by siltstone and mudstone (>85%) with minor amounts of interbedded carbonate and sandstone (Ford and Breed, 1973; Dehler et al., 2001). Until recently, the Chuar Group was composed of just the Galeros and Kwagunt formations (Ford and Breed, 1973). The Nankoweap Formation, a ~100 m thick succession of dominantly quartz arenite and interbedded red siltstone and shale, was recently added to the basal Chuar Group based upon a U-Pb detrital zircon maximum depositional age of ca. 782 Ma (Dehler et al., 2017). The Nankoweap Formation consists predominantly of siliciclastic strata

deposited in shallow water environments. Above the Nankoweap Formation, the overlying Galeros Formation has been divided into the Tanner, Jupiter, Carbon Canyon, and Duppa members. These units consist predominantly of meter-scale cycles of variegated mudstone, siltstone and sandstone capped with carbonate (primarily dolomite) and abundant evidence of desiccation including mud cracks, consistent with deposition in a restricted or marginal marine environment (Dehler et al., 2001). The overlying Carbon Butte Member, which forms the base of the Kwagunt Formation, consists of red-weathering sandstone within broad channel forms, which contain sedimentary features indicative of a wave- and possibly tide-influenced setting (Dehler et al., 2001). Above the Carbon Butte Member, the Awatubi and Walcott members consist of thick intervals of dark mudstone with minor dolomite. These were deposited in relatively deeper water than the underlying middle Chuar units following a significant basin deepening and a marine transgression. This interpretation is supported by the lack of wave generated bedding structures, the decrease of nearly ubiquitous meter-scale cycles and exposure surface as in the underlying Galeros Formation, the greater total organic carbon (TOC) content, and an increased presence of sulfides (Dehler et al., 2001; 2005; Johnston et al., 2010; Lillis, 2016; Table 1).

Fe-speciation studies reveal periods of ferruginous bottom water conditions throughout deposition of the Chuar Group, and, along with elemental Mo data and S-isotope analyses, eutrophication and the development of sulfidic water columns during late Walcott time, which has been interpreted to be the result of local organic carbon loading (Canfield et al., 2008; Nagy et al., 2009; Johnston et al., 2010; Dahl et al., 2011). Large (>2 cm diameter) marcasite nodules (FeS₂, the predominant dimorph of pyrite in depositional settings with pH <5) were sampled for Re-Os sulfide geochronology (Fig. 4). Experimental studies have shown that marcasite in marine sediments likely forms at low temperatures via nucleation and subsequent sulfidation of a monosulfide precursor, a process supported by the development of sulfide-rich (euxinic) conditions in the uppermost Chuar Group sediments (Berner, 1970; Schoonen and Barnes, 1991; Schoonen, 2004; Johnston et al., 2010).

The Chuar Group also preserves diverse microfossil assemblages, including VSMs, acritarchs with morphologically complex ornamentation, stromatolites and ciliates (Ford and Breed, 1973; Bloeser et al., 1977; Bloeser, 1985; Summons et al., 1988; Porter et al., 2003; Porter and Knoll, 2000; Porter and Riedman, 2016). Importantly, the highest acritarchs diversity

is in the Tanner and Jupiter members followed upsection by a decrease in diversity and abundance within the non- to marginal-marine upper Galeros Formation. The marine Kwagunt Formation shows a continued decline in acritarch diversity up-section followed by the appearance of vase-shaped microfossils (VSMs), beginning in the upper Awatubi Member and reaching their greatest abundance in carbonate concretions found within shale in the upper Walcott Member (Porter and Riedman, 2016). The assemblages of VSMs in the marine Kwagunt Formation are excellent candidates for biostratigraphic division of the Neoproterozoic Era (e.g. Strauss et al., 2014) due to their distinctive morphology, excellent modes of preservation, abundance ($\sim 10^6$ individuals per cm^3), global distribution and wide facies distribution coupled with a limited stratigraphic range.

Until recently, an age model for the Chuar Group was limited to an air-abrasion, upper-intercept isotope dilution-thermal ionization mass spectrometry (ID-TIMS) U-Pb zircon date of 742 ± 6 Ma from a reworked tuff, a relatively low precision ^{40}Ar - ^{39}Ar date on marcasite nodules, a <782 Ma maximum depositional age of the Nankoweap Formation based on detrital zircons, and chemostratigraphic and lithostratigraphic correlations to other Tonian successions (Karlstrom et al., 2000; Dehler et al., 2017). A new chemical abrasion ID-TIMS age for this tuff and the new Re-Os ages presented here better temporally constrain the strata of the Chuar Group and the biotic, geochemical, tectonic, and climatic records hosted within them.

SAMPLES AND ANALYTICAL METHODS

Total Organic Carbon analysis

The weight percent of Total Organic Carbon (TOC) and carbonate content for the Walcott, Carbon Canyon and Tanner members were generated from combustion of powdered samples using a LECO 244 carbon analyzer at GeoMark Research Laboratories, Houston, Texas.

U-Pb zircon geochronology

The volcanic tuff at the top of the Walcott Member of the Kwagunt Formation previously dated as 742 ± 6 Ma (Karlstrom et al., 200) was resampled (EGC1) during the 2012 field season. The ash is 1.1 m below the basal contact of the Sixtymile Formation. Sample EGC1 was washed with a deflocculant and a sonicator at the MIT geochronology lab. Zircon grains were picked under a stereoscopic light microscope, annealed in a muffle oven, and mounted at Harvard

University. Cathodoluminescence (CL) imaging, followed by tandem LA-ICPMS and CA-ID-TIMS analyses on the same zircon crystals were completed in the Isotope Geology Laboratory at Boise State University using the methods described in Rivera et al. (2013; 2016).

Uncertainties on U-Pb isotope ratios and dates are reported at the 95% confidence interval (2σ) in Table 2. Uncertainties on the weighted mean date reported for the Walcott Member tuff are given as $\pm x$ (y) [z], where x is the internal error based on analytical uncertainties only, including counting statistics, subtraction of tracer solution, and blank and initial common Pb subtraction, y includes the tracer calibration uncertainty propagated in quadrature, and z includes the ^{238}U decay constant uncertainty propagated in quadrature. The latter uncertainty should be considered when comparing our dates with those derived from other chronometers e.g., the ^{187}Re - ^{187}Os decay scheme (Schoene et al., 2006).

Marcasite nodule and sedimentary rock Re-Os geochronology

Samples collected during the 2014 field season for Re-Os sedimentary geochronology include: dark grey calcareous dolomite from the basal Tanner Member in Basalt Canyon (A1408); dark grey dolomite from the middle Carbon Canyon Member in Carbon Canyon (A1407); marcasite nodules within black shale of the Awatubi Member at Nankoweap Butte (marcasite nodules 1-5); and dark grey-black shale from the top of the Walcott Member at Nankoweap Butte (A1402; Fig. 2). Samples (A1402) of the Walcott Member were collected 11 m below the 742 ± 6 Ma ash and along a lateral interval of 10.7 m and a vertical interval of 43 cm (All coordinates for sample sites are in Table 1). Samples of the Walcott Member were collected from trenches dug 0.8 m into the hillside in an attempt to avoid oxidative surficial weathering; a process that has been shown to disturb the Re-Os geochronometer (Jaffe et al., 2002; Kendall et al., 2009a, b; Rooney et al., 2011; Georgiev et al., 2012). Five large (>200 g per sample) samples of the Carbon Canyon Member (A1407) were collected 215 m above the contact with the underlying Jupiter Member, along strike over 4.3 m and within a 17 cm vertical interval. Eight large (>100 g) samples were collected 19.7 m above the base of the Tanner Member (A1408) laterally over 4.2 m and a vertical interval of 19 cm with the aim of providing a maximum depositional age for sedimentation of the Galeros Formation. Five large (>2 cm diameter) marcasite nodules were collected ~ 3 m above *Boxonia-Baicalia* stromatolites of the basal section of the Awatubi Member along strike over an interval ~ 8 m.

To expose the freshest surfaces possible, samples were trimmed using a diamond-edge rock saw and then hand-polished using a diamond-encrusted polishing pad to remove cutting marks and eliminate any potential for metal contamination from the saw blade. Samples A1407-B, -C and -D were large enough to be split in half (i.e., B and Bii) and do not represent replicate analyses. The sedimentary samples were dried overnight at ~60°C and then crushed to a fine (~100 µm) powder in a SPEX 8500 Shatterbox using a zirconium ceramic grinding container and puck in order to homogenize any Re and Os heterogeneity present in the samples (e.g., Kendall et al., 2009a).

The Cr^{VI}O₃-H₂SO₄ digestion method was employed for Re-Os analysis of the organic-rich sedimentary units because this method has been shown to preferentially liberate hydrogenous Re and Os without leaching the detrital budget and thus yield more accurate and precise dates (Selby and Creaser, 2003; Kendall et al., 2004; Selby et al., 2009; Rooney et al., 2011). Sedimentary sample powders weighing 0.9-0.93 g together with a mixed tracer (spike) solution enriched in ¹⁹⁰Os and ¹⁸⁵Re were dissolved in 10 ml of a Cr^{VI}O₃-H₂SO₄ solution (0.25g/g Cr^{VI}O₃ in 4N H₂SO₄) in a sealed carius tube for 48 hours at 220°C. Marcasite nodules were crushed using a ceramic mortar and pestle. An aliquot (~0.4 g) of marcasite was loaded into a carius tube with a known amount of mixed ¹⁹⁰Os and ¹⁸⁵Re spike and digested using inverse *aqua regia* (6 ml of 16 N HNO₃ and 3 ml of 12 N HCl) for 48 hours at 220°C.

Rhenium and Os isotope analyses of the organic-rich sedimentary units and marcasite followed methods outlined in Selby and Creaser (2003) and Selby et al. (2009), respectively. Osmium was isolated using solvent extraction using CHCl₃, back-extracted by HBr, and further purified using micro-distillation. The Re of the resultant Os extracted solution were isolated and purified using NaOH-(CH₃)₂CO solvent extraction and anion column chromatography methods (Selby and Creaser, 2003; Cumming et al., 2013). All Re and Os isotopic measurements were determined by negative TIMS (Creaser et al., 1991; Völkening et al., 1991) at the Durham University Laboratory for Source Rock and Sulfide Geochronology and Geochemistry (a member of the Durham Geochemistry Centre). The purified Re and Os fractions were loaded onto Ni and Pt filaments, respectively (Selby, 2007), with the isotopic measurements performed using a Thermo Electron TRITON mass spectrometer via static Faraday collection for Re and ion-counting using a secondary electron multiplier in peak-hopping mode for Os. For the Cr^{VI}O₃-H₂SO₄ solution total procedural blanks during this study were 16.0 ± 3.0 pg and 0.25 ±

0.05 pg (1 S.D., n = 3) for Re and Os, respectively, with an average $^{187}\text{Os}/^{188}\text{Os}$ value of 0.19 ± 0.15 (n = 3). For the inverse *aqua regia* method, procedural blanks were 3.0 ± 0.1 pg and 0.20 ± 0.1 pg (1 S.D., n = 2) for Re and Os, respectively, with an average $^{187}\text{Os}/^{188}\text{Os}$ value of 0.17 ± 0.15 (n = 2).

Uncertainties for $^{187}\text{Re}/^{188}\text{Os}$ and $^{187}\text{Os}/^{188}\text{Os}$ were determined by propagation of all uncertainties in Re and Os mass spectrometer measurements, blank abundances and isotopic compositions, spike calibrations and reproducibility of standard Re and Os isotopic values. The Re–Os isotopic data including the 2σ propagated uncertainties for $^{187}\text{Re}/^{188}\text{Os}$ and $^{187}\text{Os}/^{188}\text{Os}$ and the associated error correlation function (ρ) were used to calculate a Re–Os isochron date using Isoplot V. 4.15 and the λ ^{187}Re constant of $1.666 \times 10^{-11} \text{a}^{-1}$ (Ludwig, 2009; Smoliar et al., 1996). Final age uncertainty includes the uncertainty in the decay constant, which permits a direct comparison with the U–Pb date of this study. As a monitor of mass spectrometry reproducibility, two in-house Re and Os standard solutions were analyzed (Re std and Durham Romil Osmium Standard = DROsS, respectively). The Re standard yields an average $^{185}\text{Re}/^{187}\text{Re}$ ratio of 0.5979 ± 0.0004 (1 S.D., n = 8) and the Os standard gave a $^{187}\text{Os}/^{188}\text{Os}$ ratio of 0.16089 ± 0.00055 (1 S.D., n = 7), both of which are in agreement with previous studies (Finlay et al., 2010; Rooney et al., 2010).

RESULTS

TOC and carbonate abundance

Samples from the Walcott, Carbon Canyon and Tanner members have average carbonate contents of 81.3, 89.8 and 79.3 wt.%, respectively (Table 1). The average TOC values for these units are 0.61, 0.11 and 0.55 wt.%, respectively and all organic matter indices are comparable with those reported by Lillis (2016; Table 1).

Organic-rich shale and carbonate samples of the Tanner, Carbon Canyon and Walcott members

Elemental Re and Os abundances for organic-rich dolomite of the Carbon Canyon Member (A1407 samples) range from 0.5 to 2.9 ng/g and 42.9 to 151.3 pg/g, respectively, and are moderately elevated in comparison with average upper continental crust values of 1 ng/g and 50 pg/g, respectively (Table 3; Esser and Turekian, 1993; Peucker-Ehrenbrink and Jahn, 2001;

Hattori et al., 2003; Sun et al., 2003). The A1407 samples have $^{187}\text{Re}/^{188}\text{Os}$ and $^{187}\text{Os}/^{188}\text{Os}$ values that range from 16.5 to 324.3 and 1.333 to 5.226, respectively, (Table 3). Regression of the isotopic composition data yield a Model 1 date of 757.0 ± 6.6 (6.8) Ma (2σ , bracketed age uncertainty includes the ^{187}Re decay constant uncertainty, λ , $\sigma_\lambda = 0.175\%$ of λ , $n = 8$, Mean Square Weighted Deviation [MSWD] = 0.47), with an initial $^{187}\text{Os}/^{188}\text{Os}$ [Osi] value of 1.13 ± 0.02 (Fig. 5A).

Samples of the Walcott and Tanner members did not yield isochronous dates, although enriched in both Re and Os (Table 3). The Walcott Member samples (A1402) have elemental Re and Os abundances from 11.0 to 75.4 ng/g and 163 to 238 pg/g, respectively. The $^{187}\text{Re}/^{188}\text{Os}$ and $^{187}\text{Os}/^{188}\text{Os}$ values for the Walcott Member samples range from 375.7 to 2400.2 and 2.475 to 4.164, respectively (Table 3). Organic-rich dolomite from the Tanner Member have Re and Os abundances that range from 4.4 to 24.3 ng/g and 18.4 to 28.4 pg/g, respectively, and possess $^{187}\text{Re}/^{188}\text{Os}$ and $^{187}\text{Os}/^{188}\text{Os}$ values from 1904 to 9484 and 10.06 to 10.13, respectively. For the Walcott Member calculated Osi values at 740 Ma yield nonsensical and highly subchondritic values from -2.1 to -25.6; the Tanner Member Osi at 770 Ma range from -14.4 to -112.3 (Table 3).

Marcasite nodules of the Awatubi Member

Marcasite nodules from the Awatubi Member have elemental Re and Os abundances ranging from 3.1 to 4.8 ng/g and 161 to 289 pg/g, respectively. The $^{187}\text{Re}/^{188}\text{Os}$ and $^{187}\text{Os}/^{188}\text{Os}$ values are between 66.1 and 132.7 and 1.270 and 2.103, respectively (Table 3). Regression of the isotopic composition data yield a Model 1 date of 751.0 ± 7.2 Ma (7.6) (2σ , $n = 5$, MSWD = 0.37), with an Osi value of 0.44 ± 0.01 (Fig. 5B)

Walcott Member tuff geochronology

Cathodoluminescence imaging of the zircon crystals separated from the upper Walcott Member tuff revealed a dominant population of brightly luminescent grains exhibiting muted sector and oscillatory zonation, as well as a minority of dark non-luminescent grains with more distinct oscillatory zoning (Fig. 6). In situ LA-ICPMS spot analyses on these grains yielded Neoproterozoic dates for the dominant luminescent grains (Table S1) and low actinide and lanthanide contents (Table S2) consistent with their bright CL response. Some spots on the CL-

bright grains gave discordant and older apparent U-Pb dates correlated with elevated signals at mass 204, indicative of the intersection of common Pb-bearing glass and/or feldspar inclusions. Two CL-dark grains gave concordant dates of 1.4 and 1.1 Ga and are clearly reworked inherited grains.

Based upon CL imagery and LA-ICPMS results, a selection of eight grains were plucked from the epoxy mounts and analyzed via CA-IDTIMS (Table 2). All grains yield concordant and equivalent isotope ratios with a weighted mean $^{206}\text{Pb}/^{238}\text{U}$ date of $729.00 \pm 0.27(0.44)$ [0.86] Ma. Given the consistency of this result and the simplicity of the zoning and compositions of this population of zircons, we interpret this result as the best estimation, within its analytical uncertainty, of the eruption and depositional age of the tuff.

DISCUSSION

Correlation of late-Tonian basins across Western Laurentia

Our new ^{206}Pb - ^{238}U zircon age of 729.0 ± 0.9 Ma (MSWD = 0.86) from the uppermost Walcott Member of the Kwagunt Formation improves correlation with other Chuar-equivalent Neoproterozoic basins across western Laurentia. This refined CA-ID-TIMS age differs from the older air abrasion age of 742 ± 6 Ma by >10 million years, decreasing the upper age constraints on pre-Cryogenian basin formation across the western USA. Our new U-Pb and Re-Os ages for the Chuar Group is consistent with the sedimentation history of the Mount Harper Group as indicated by the close agreement with a Re-Os age of 732.2 ± 4.7 Ma from the Callison Lake Formation (Rooney et al., 2014).

Sedimentation history and depositional environment of the Chuar Group

The new U-Pb and Re-Os geochronology data for the Carbon Canyon Member and marcasite nodules of the Awatubi Member provide much-needed age constraints for the Chuar Group. These dates improve existing lithological and chemostratigraphic correlations with Tonian strata of western North America and other globally documented examples of VSMs (Karlstrom et al., 2000; Porter and Knoll, 2000; Porter et al., 2003; Dehler et al., 2010; Macdonald et al., 2010; 2013; Mahon et al., 2014; Strauss et al., 2014; Riedman and Porter, 2016; Fig. 3).

Our new ^{206}Pb - ^{238}U zircon age of 729.0 ± 0.9 Ma from the tuff within the Walcott Member extends the duration of Chuar Group sedimentation by more than 10 Myr, and the known range of VSM also by ~ 10 Myr, thus shortening the apparent interval between VSM-rich horizons and the first Cryogenian glaciation to ~ 12 Myr. The significant revision of this U-Pb zircon age (reduced by ~ 12 Myrs) compared to the interpretation of Karlstrom et al. (2000) results from the ability of the chemical abrasion method to selectively remove Pb-loss domains from the zircon crystals, resulting in concordant and equivalent results for each residual crystal. This allows the relatively simple and robust interpretation of the age of the tuff from the weighted mean of the ^{206}Pb - ^{238}U dates, and obviates the need to rely on the upper intercept of a discordia line, which is prone to inaccuracy for Neoproterozoic zircons due to the slight angle between that regression and the concordia curve, and a small bias in the historically utilized $^{235}\text{U}/^{238}\text{U}$ decay constant ratio (Condon and Bowring, 2011; Schmitz, 2012).

The 756.0 ± 6.8 Ma Re-Os date for the Carbon Canyon Member provides a maximum age constraint for the first appearance datum of VSMs in the overlying Kwagunt Formation (e.g., Porter and Knoll, 2000; Strauss et al., 2014). This fossil assemblage contains the first evidence for predation amongst eukaryotes, (“eukaryvory”; Porter, 2011; Knoll, 2014). The 751.0 ± 7.6 Ma Re-Os date from marcasite nodules of the Awatubi Member provides an age of nodule growth at or near the sediment-water column interface prior to compaction and lithification, an interpretation supported by thickening of mudstone laminae at the edges of the nodules. This age is more precise than the $^{40}\text{Ar}/^{39}\text{Ar}$ date of 764 ± 16 Ma (this uncertainty does not include the uncertainty on ^{40}K) on a marcasite nodule from the same bed reported by Dehler et al. (2017) and is considered to be more accurate because of uncertainty in the origin of the parent potassium in the marcasite.

The *Osi* data presented here provides further support for the transition from a restricted depositional setting of the middle Chuar Group to one with greater connectivity to the global ocean as recorded in unique sterane distributions found in the upper Chuar Group (Summons et al., 1988; Brocks et al., 2016). The Os isotope composition of seawater at the time of deposition of sediment is interpreted to reflect an input balance between radiogenic sources ($^{187}\text{Os}/^{188}\text{Os} \sim 1.4$; weathering of upper continental crust via riverine input) and unradiogenic sources ($^{187}\text{Os}/^{188}\text{Os} \sim 0.13$; cosmic dust, hydrothermal fluids and weathering of mafic or ultramafic rocks) with a modern day Os isotope composition of ~ 1.06 (Sharma et al., 1997; Levasseur et al.,

1998; Woodhouse et al., 1999; Peucker-Ehrenbrink and Ravizza, 2000). Although the sample set is small ($n < 20$), the majority of Neoproterozoic Osi values are generally unradiogenic (< 1.0) (with the exception of values from post-Sturtian and post-Marinoan transgressive successions) indicating that the Neoproterozoic Os isotope composition of marine waters was largely unradiogenic (Rooney et al., 2015). In contrast, the highly radiogenic Osi value (1.13) of the Carbon Canyon Member is indicative of increased weathering from continental sources and/or a reduction in weathering of juvenile lithologies as has been described in Phanerozoic settings indicative of lacustrine-oceanic transitions (Poirier and Hillaire-Marcel, 2011; Cumming et al., 2013; Xu et al., 2017). Although not definitive, the highly radiogenic Osi signal reported here supports sedimentological and acritarch data that suggest the strata of the middle Chuar Group may have been deposited in a non-marine to restricted basin setting (*c.f.*, Dehler et al., 2001; Porter and Riedman, 2016). Further, the upper Galeros Formation siliciclastic strata displays black to green to red color changes that track grain size—a characteristic of Van Houten cycles and Newark type lacustrine facies complexes (Olsen, 1990). In contrast, these restricted facies assemblages of the middle Chuar Group disappear with the transgressive sequence in the overlying Kwagunt Formation, which is accompanied by the appearance of sulfide nodules, presumably sourced from sulfate-laden seawater, in the Awatubi Member with Osi values of ~ 0.44 . Thus, we suggest that chemostratigraphic and biostratigraphic changes through the Chuar Group be interpreted through the lens of local environmental change from non-marine to a marine setting rather than changes in global marine geochemistry and ecology (*c.f.*, Corsetti et al., 2009; Nagy et al., 2009).

Re-Os geochronology isotope systematics and treatment and evaluation of Re-Os isotope data

Physical and chemical weathering disturbance of the Re-Os system

Building upon advances in sampling, analytical, and chemical isolation and purification techniques numerous studies have shown that the Re-Os geochronometer is a robust technique capable of providing accurate depositional ages for sedimentary strata that have experienced hydrocarbon maturation events, greenschist facies metamorphism, and flash pyrolysis, suggesting the system is robust even at temperatures and pressures $> 350^\circ\text{C}$ and ~ 3 kbar (Creaser et al., 2002; Selby and Creaser, 2005; Kendall et al., 2004, 2006, 2009b; Yang et al., 2009;

Rooney et al., 2010, 2011; Georgiev, et al., 2011). In contrast, previous studies have revealed that both oxidative weathering (Peucker-Ehrenbrink and Jahn, 1998; Peucker-Ehrenbrink and Hannigan, 2000; Jaffe et al., 2002; Pierson-Wickmann et al., 2002; Georgiev et al., 2012) and hydrothermal fluid flow (Kendall et al., 2009b; Rooney et al., 2011) can result in post-depositional disturbance of the Re-Os geochronometer.

Organic-rich shales from outcrop exposures of the Walcott and Tanner members were sampled in an identical fashion (removal of surficial weathering, taking large ~100 g samples and avoiding any visible alteration e.g., veining) to those of the Carbon Canyon Member so we do not consider sampling methods to have resulted in disturbance of Re-Os systematics in the Walcott and Tanner members. Samples of the Walcott and Tanner members have elevated Re abundances ranging from 4.4 ng/g to 75 ng/g, but do not have correspondingly high Os abundances as would be expected from the decay of significant amounts of Re (several ng/g) to radiogenic ^{187}Os over an interval of ~740 Myr (Table 3). Addition of Re or loss of Os are two processes that would explain the disturbance of these samples in contrast with those of the Carbon Canyon Member. Loss of Re and Platinum Group Elements (PGEs) has been identified from outcrop samples of Late Ordovician shales and was attributed to oxidation of organic matter (OM; Peucker-Ehrenbrink and Hannigan, 2000). However, lacking a mechanism capable of *only* adding Re to the kerogen component of sedimentary rocks we suggest that the depleted levels of Os in the Walcott and Tanner samples occurred geologically recently. This depletion could be the result of flushing with CO₂-rich brines from nearby Paleocene intrusives resulting in oxidative weathering of labile OM and the liberation of Os from these samples (Lillis, 2016).

Re-Os geochronology and data evaluation: isochron ages are not axiomatically accurate

A number of studies have established the organophilic behavior of Re and Os and its uptake in OM, primarily under anoxic conditions (Ravizza et al., 1991; Ravizza and Turekian, 1992; Colodner et al., 1993; Crusius and Thomson, 2000). Pioneering work by Ravizza and Turekian (1989) using the Re-Os geochronometer to accurately date the Bakken Shale of North America highlighted the potential of the Re-Os system to deliver vital information on the sedimentary rock record. This capability was further highlighted by Re-Os studies of both hydrocarbon immature Jurassic strata of the UK (Cohen et al., 1999) and hydrocarbon mature Devonian Strata of Canada (Creaser et al., 2002). An early study by Schafer and Burgess (2003)

highlighted the impact of detrital Os liberated from the silicate matrix when employing inverse *aqua regia* for sample digestion that resulted in anomalously young ages. Development of chromic acid ($\text{Cr}^{\text{VI}}\text{O}_3\text{--H}_2\text{SO}_4$) for digestion of organic-rich sedimentary samples demonstrated the advantages of preferentially liberating the hydrogenous (seawater derived) Re and Os associated with OM resulting in accurate *and* more precise ($<0.5\%$ uncertainty) age determinations (e.g., Selby and Creaser, 2003; Kendall et al., 2004; 2006).

Data regression and Model 1, 2 or 3 ages of isochrons

The Re-Os geochronometer utilizes the isochron technique whereby radiogenic isotopes for co-genetic samples are plotted against the parent/daughter ratio (e.g., $^{187}\text{Os}/^{188}\text{Os}$ vs. $^{187}\text{Re}/^{188}\text{Os}$) forming a best-fit line or isochron. The slope of this line is proportional to the age with the y-intercept representing the initial Os isotope composition of seawater at the time of deposition (isochron generated age). Inherent in this treatment of the Re-Os data are several assumptions: 1) the Re and Os measured are predominantly hydrogenous in origin; 2) the Re-Os systematics of the samples have not been disturbed since chelation of Re and Os during deposition and; 3) the initial Os isotope composition of seawater at the time of deposition represented by the samples analyzed was homogenous. Generation of an isochron does not automatically signify that the age is reliable; the accuracy of isochron ages is not axiomatic (Zheng et al., 1989; *c.f.* Spence et al., 2016).

Additional factors related to the uncertainties and errors associated with the measured Re and Os data are considered in the linear regression algorithms (York, 1969) and software (Isoplot V. 4.15; Ludwig, 2009), and are presented as a Model classification (1, 2 or 3) and a reduced χ^2 parameter often referred to in the geological literature as the MSWD (*c.f.* Wendt and Carl, 1991). In order to assess the accuracy of an age, the MSWD and Model classification should be presented to aid the reader in their assessment of the fidelity of the age presented. The Model 1 age represents a fit of a line to the data with the assigned analytical errors representing scatter from the best-fitting line. Assigning equal weights and zero error-correlations to each data point generates Model 2 ages. This regression avoids weighting the points according to analytical uncertainties when the misfit is larger than what is predicted from analytical error (*c.f.* Model 1). A Model 3 age assumes that the scatter on the isochron is due to a combination of assigned analytical uncertainty and a normally distributed uncertainty around the Model 1 based initial

isotope ratios (Ludwig, 2003), with the age uncertainty expanded from internal uncertainty by the square root of the MSWD and Student's t multiplier for the associated degrees of freedom. All ages discussed in this study are Model 1 ages as the age data do not require the assumption of uncertainty in the initial isotope ratios.

The MSWD is a measure of goodness of fit that quantifies whether or not the data, within their uncertainty, are consistent with the best-fitting line. A poor fit can therefore imply that the data do not fall on a common line due to differences in the initial Os composition, or that the assigned uncertainties are inadequate, or the samples are not of the same age. The calculation weights the deviation for each data point from the best-fit line by its uncertainty, which will result in an MSWD of ~ 1 if these deviations are on the order of the uncertainty. The formulation of the MSWD takes the covariance between data into account (McDougall and Harrison, 1999). A calculated MSWD $\gg 1$ suggests that the data are too far away from a best-fit line or that the uncertainties prescribed were underestimated. In contrast, an MSWD $\ll 1$ indicates that the data are very close to the best-fit line, either due to overestimation of analytical uncertainties or unrecognized error correlations.

Uncertainties and error propagation of Re-Os geochronology datasets

For the propagation of uncertainties into the estimated individual Re and Os ratios we use the common error propagation approximation that results from the first order (linearized) Taylor series expansion of a function around its variables (e.g. Bevington and Robinson, 1992; Equation 1):

$$\sigma_f^2 = \left(\frac{\partial f(x,y,\dots)}{\partial x}\right)^2 \cdot \sigma_x^2 + \left(\frac{\partial f(x,y,\dots)}{\partial y}\right)^2 \cdot \sigma_y^2 + \left(\frac{\partial f(x,y,\dots)}{\partial x}\right)\left(\frac{\partial f(x,y,\dots)}{\partial y}\right) \cdot 2\sigma_{xy}^2 + \dots \quad (1)$$

where σ_f^2 is the variance of f , σ_{xy}^2 is the covariance between the variables x and y and $\partial f/\partial x$ is the first partial derivative of f with respect to x . When propagating uncertainties into the $^{187}\text{Re}/^{188}\text{Os}$ and $^{187}\text{Os}/^{188}\text{Os}$ values we assume that the different contributions (see Fig. 8) are independent from each other, hence their covariance is zero. As an example, the uncertainty in the $^{187}\text{Os}/^{188}\text{Os}$ isotope ratio is given by:

$$\sigma_{\frac{^{187}\text{Os}}{^{188}\text{Os}}}^2 = \left(\frac{1}{^{188}\text{Os}}\right)^2 \cdot \sigma_{^{187}\text{Os}}^2 + \left(\frac{^{187}\text{Os}}{^{188}\text{Os}^2}\right)^2 \cdot \sigma_{^{188}\text{Os}}^2 \quad (2)$$

The full set of equations to propagate uncertainties in the Re-Os system can found in Isoplot (Ludwig, 2009).

The resulting uncertainties for the two ratios will, however, covary as both isotopes (^{187}Re and ^{187}Os) are taken relative to the same isotope (^{188}Os). Therefore, to calculate an age from the different isotope ratios we take this into account by performing a linear regression that includes the uncertainties in the Re and Os ratios and their covariance following the approach by York et al. (2004).

In an effort to improve the precision of the age we analyzed the magnitude with which different sources of uncertainty propagate into the final age uncertainty following the approach taken by Schmitz and Schoene (2007) for ID-TIMS U-Pb analyses. This allows us to strategically target those procedures that contribute most to the age uncertainty and improve them in future work. We highlight however that the analysis below only applies to the presented dataset. We assess contributions to the age uncertainty by looking at how much it is reduced if individual contributing uncertainties are reduced. Figure 8A shows the age uncertainty (y-axis) decrease if the uncertainty in individual contributors to the age uncertainty (x-axis) is reduced by 25%. Uncertainties can be systematic (green markers) or random (blue markers). The uncertainty in half-life (red marker) does not influence the best-fitting isochron and is therefore considered separately. Panel A shows that the half-life uncertainty, the mixed Re-Os spike weight uncertainty and the ^{190}Os spike calibration uncertainty contribute most to the age uncertainty. Reducing them individually leads to an age uncertainty that is reduced by 3.4%, 3.4% and 4.1% respectively (age uncertainties are reduced to 6.55, 6.55 and 6.50 Ma, instead of the current 6.78 Ma; Fig. 8). Again, we caution that these values are only valid for the dataset presented here and may vary for the analysis of other datasets. Panel B shows that an increasing precision in the different terms leads to a MSWD that is closer to 1, i.e. the data and their uncertainties tend to be more consistent with the determined best-fit line. Conceptually, an underestimation of analytical uncertainties can lead to a very poor fit to a single isochron, which would then require geological conditions to invoke other uncertainties for example differences in the initial Os isotope composition of seawater to explain the variability in the data. Accounting for this additional uncertainty would result in a Model 3 age. However, we note that in our dataset, the initial MSWD is 0.47 making the data already more compatible with the isochron than their uncertainties would suggest. Therefore, reducing the input uncertainties (e.g. by 25% as we do here) leads to an improved MSWD and does therefore not lead to a Model 3 age.

Another possibility of decreasing the age uncertainty is by increasing the mixed ^{185}Re - ^{190}Os spike weight. For example, increasing it by 25% would lead to a decrease in age uncertainty by 4.7% (to 6.46 Ma). Note that increasing the spike weight would likely also require an alteration of the spike concentration, which was not considered here.

As discussed above, the uncertainty from the Model 3 regression is treated differently from that of a Model 1 regression. An underestimation of analytical uncertainties can lead to Model 3 ages when the probability of fit is low. In our uncertainty evaluation above, although the uncertainties are reduced significantly (e.g., 25 %), the probability of fit is maintained and suggests that with the current analytical precision, there is potential to further improve the precision of the isochron age.

These results are highly dataset dependent and to demonstrate that figures 8C and D show the same considerations of reducing uncertainties in the individual contributions but only for 6 of the 8 samples (excluding samples A1407C and Cii). This exclusion leads to a smaller range in isotope ratios (*c.f.* Fig. 5A) and therefore increases the age uncertainty significantly (to 15.54 Ma). This illustrates that the uncertainty in the age is not only controlled by uncertainties related to the measurement but also by the spread in the obtained Re-Os data. It will also lead to a different result regarding which process contributes most to the age uncertainty, despite the fact that most of the input uncertainties are identical among the different samples. This highlights the non-linearity of the regression, which incorporates the covariance between the different samples and underlines the need for including the error correlation function.

Next, we consider how the uncertainties in the isotope ratios generated over the course of an analytical session for one sample (*e.g.*, 100 ratios on the Secondary Electron Multiplier for Os isotopes) propagate into the final age uncertainty. Figure 9A shows the uncertainty in the mean $^{187}\text{Os}/^{188}\text{Os}$ ratio (*i.e.* the standard error) for an increasing number of measurements for each sample. As expected, the measurement uncertainty improves with an increasing number of measurements per sample. The diamond at the highest number of measurements corresponds to the uncertainty used to calculate the age described in this paper. To estimate how the uncertainty would improve if we were able to increase the number of measurements we fitted a double exponential curve to each sample and extrapolated the uncertainty to 150 measurements (grey lines). In Figure 9B we repeat the calculations for the uncertainty in the measured $^{190}\text{Os}/^{188}\text{Os}$. We continue to use the individual uncertainties as well as the uncertainties obtained from the

fitted curves to calculate the covariance (ρ), the resulting MSWD (Fig. 9C) and age uncertainty (Fig. 9D). This uncertainty correlation function (ρ) is included because our uncertainties are highly correlated (e.g., Cumming, 1969; York, 1969; Ludwig, 1980; Morelli et al., 2005). It is important to note that the MSWD and age uncertainty are therefore not extrapolated but rather calculated self-consistently from the extrapolated uncertainties in the isotope ratios (Figs. 9A and B). Following the estimate curves shows that increasing the number of measurements per sample to 150 would reduce the age uncertainty by 10% (to 6.1 Ma) and increase the MSWD to 0.49. Compared to the changes in uncertainty introduced by the other components described above, for this specific dataset increasing the number of measurements or increasing beam stability or the use of multiple ion counters may be the most efficient ways of reducing uncertainties in the obtained age. Note that any of these changes described in this section would not only affect the age uncertainty, but also the age itself.

CONCLUSIONS

A thorough analysis of the uncertainty propagation provides insight into future improvements in the precision of the Re-Os geochronometer. For the samples from the basal Carbon Canyon Member we found that reducing the random uncertainty in the mixed Re-Os spike weight and the systematic uncertainty in the ^{190}Os spike calibration provide a means for improving the precision of the age estimate. Samples from the Walcott and Tanner members of the Chuar Group failed to yield meaningful ages despite elevated Re enrichments (>20 ng/g). The Re-Os data from these units yield negative Osi values, which suggests disturbance to the Re-Os systematics. The low Os abundances (typically <100 pg/g) relative to the amount expected based on the Re abundance, suggest leaching of Os through oxidative weathering.

Our new sedimentary rock Re-Os data from the Carbon Canyon Member of the Galeros Formation yield a depositional age of 756.0 ± 6.8 Ma. The Osi value (1.13) for the Carbon Canyon Member indicates that the Os flux was dominated by weathering of the upper continental crust with minimal contribution from hydrothermal or seafloor alteration sources suggestive of a restricted marine basin. This geochemical signal is consistent with the non- to marginal-marine facies assemblage in the Galeros Formation. Application of Re-Os sulfide geochronology to marcasite nodules from the fossiliferous Awatubi Member yields an age of 751.0 ± 7.6 Ma and is interpreted to reflect the best estimate of the depositional age for this unit and maximum age

constraint for the VSM assemblages from this unit. The $^{187}\text{Os}/^{188}\text{Os}$ value of 0.44 for these nodules along with the disappearance of non-marginal facies assemblages, and the appearance of sulfides within a broad transgressive sequence, are consistent with a major marine incursion between the Galeros and Kwagunt formations. The recognition of these local environmental changes in the Chuar basin provides much-needed context for existing biostratigraphic, chemostratigraphic, and biomarker data. These new Re-Os ages from the Chuar Group and our refined age of the tuff in the upper Walcott Member of the Kwagunt Formation at 729.0 ± 0.9 Ma further enhance correlations with other mid-Neoproterozoic strata of western North America and support a limited stratigraphic range (<20 Myr) for these microfossils.

FIGURE CAPTIONS

Figure 1: Location map showing outcrop extent of the Grand Canyon Supergroup and major tectonic elements in eastern Grand Canyon. ck-Creek (modified from Timmons et al., 2001; online version in color).

Figure 2: Generalized stratigraphic column of the Chuar Group, showing relationships with underlying and overlying units modified from Dehler et al. (2001). Ages are from: (1) this paper; (2) Dehler et al., 2017. Nank-Nankoweap; Du-Duppa Member; CB-Carbon Butte (Online version in color). VSMs are from Porter and Knoll, 2000.

Figure 3: Correlation of Chuar Group stratigraphy with other Neoproterozoic strata of western North America. Age constraints are from: (1) Macdonald et al., 2010; (2) Strauss et al., 2014; (3) Rooney et al., 2015; (4) Rooney et al., 2014; (5) Mahon et al., 2014; (6) Dehler et al., 2010; (7) Hansen, 1965; (8) this paper; (9) Dehler et al., 2017. LDB-Little Dal Basalt; RCQ-Red Creek Quartzite; Pz-Paleozoic; CS-Crystal Spring; Nank-Nankoweap; Du-Duppa Member; CB-Carbon Butte; KP 1 and 2; Kingston Peak; VS-Virgin Spring. VSMs are from: Strauss et al., 2014; Horodyski, 1993; Macdonald et al., 2013; Dehler et al., 2007; Porter and Knoll, 2000. (Online version in color).

Figure 4: Radiating marcasite (FeS_2) nodule (#3 on isochron) from the Awatubi Member. Marcasite is a brittle dimorph of pyrite and has an orthorhombic crystal structure. Scale bar is 1

cm. Picture taken prior to removal of weathered exterior using diamond-encrusted polishing pad.
(Online version in color).

Figure 5: A) Re-Os isochron for the Carbon Canyon Member. All data point error ellipses are 2σ and their diameters are larger than calculated error ellipses. B) Re-Os isochron for marcasite nodules of the basal Awatubi Member. All data point error ellipses are 2σ and their diameters are larger than calculated error ellipses.

Figure 6: Cathodoluminescence imagery with superimposed LA-ICPMS spot analysis U-Pb dates for zircon crystals separated from the Walcott Member tuff. Dates are in millions of years \pm errors at 2σ ; laser spot positions are illustrated with their 25 μm diameter. Laser spot numbers below each measured date, and associated CA-ID-TIMS analysis numbers for each grain correspond to data entries in Tables S1 and 3, respectively.

Figure 7: U-Pb isotope ratio concordia diagram for zircon crystals measured in this study via chemical abrasion ID-TIMS (red ellipses), compared to the legacy air abrasion ID-TIMS data (gray ellipses) of Karlstrom et al. (2000). Illustrated in the main figure is the discordia line (solid) with its error envelope (dashed) resulting in the interpreted upper intercept date of 742 ± 6 Ma by Karlstrom et al. (2000). The inset also illustrates the weighted mean $^{207}\text{Pb}/^{206}\text{Pb}$ date of the same data set as a thick solid line, for more detailed comparison with the concordant and equivalent CA-ID-TIMS data of this study. All data point error ellipses and envelopes on the concordia curve and discordia line are illustrated at 2σ .

Figure 8: Age uncertainty (y-axis) for a variety of scenarios in which the uncertainty in different input parameters (x-axis) is reduced by 25%. Parameters that are not shown here only contribute negligibly to the age uncertainty (i.e. does not affect the age uncertainty or MSWD if reduced by 25%). Parameters are sorted by systematic (green) and random (blue) uncertainties, the half live uncertainty (red) is considered separately. A) and B) Analysis when all 8 samples are considered. C) and D) Analysis when only 6 of the 8 samples are considered (samples A1407C and Cii were excluded). The grey dashed line marks the age uncertainty without changes in the input

uncertainties. The left axis in panels A and C denotes the age uncertainty; the right axis denotes the corresponding percentage in uncertainty reduction.

Figure 9: Analysis of the effect of number of measurements on the age uncertainty and MSWD. A) and B) show the uncertainty in Os ratios for increasing number of measurements per sample (e.g. for 60 measurements we used the first 60 measurements to calculate the standard error of the mean for each sample). Diamonds are calculated from the data. The grey lines denote the best fitting double exponential curves through the data. In cases where the best fit resulted in a positive exponent for either exponential we fitted a single exponential curve. C) and D) show the MSWD and age uncertainty, respectively, that result from the measured uncertainties (diamonds) and the fitted uncertainties (grey line). The legends in panel A) and C) also apply to panel B) and D), respectively.

ACKNOWLEDGMENTS

ADR acknowledges the support of a NASA Astrobiology Institute postdoctoral fellowship. FAM thanks the NASA NAI MIT node for support. EFS thanks the National Science Foundation for support through a Graduate Research Fellowship. We thank Eben Hodgkin for help in mounting and running the zircons at Boise State Isotope Geology Laboratory, and Grand Canyon National Park for research and collecting permits to KEK that allowed the sampling. DS acknowledges the Total Endowment Fund for laboratory support for the Laboratory of Sulfide and Source Rock Geochronology and Geochemistry. Funding for the analytical infrastructure of the Boise State Isotope Geology Laboratory was provided by the National Science Foundation (NSF) Major Research Instrumentation grants EAR-0521221 and EAR-1337887, and NSF Earth Sciences Division (EAR) Instrumentation and Facilities Program grant EAR-0824974. We gratefully acknowledge helpful reviews from Jon Husson, an anonymous reviewer and editorial comments from Brad Singer and Bradley Cramer.

REFERENCES CITED

Berner, R. A., 1970, Sedimentary pyrite formation: *American Journal of Science*, v. 268, p. 1-23.
Bevington, P. R., and Robinson, D. K. 1992. *Data Reduction and Error Analysis for the Physical Sciences*, 2nd ed., 328 pp., McGraw-Hill, New York.

- Bloeser, B., 1985, *Melanocyrrillium*, a new genus of structurally complex late Proterozoic microfossils from the Kwagunt Formation (Chuar Group), Grand Canyon, Arizona: *Journal of Paleontology*, p. 741-765.
- Bloeser, B., Schopf, J. W., Horodyski, R. J., and Breed, W. J., 1977, Chitinozoans from the late Precambrian Chuar group of the Grand Canyon, Arizona: *Science*, v. 195, p. 676-679.
- Brocks, J. J., Jarrett, A. J., Sirantoine, E., Kenig, F., Moczydlowska, M., Porter, S., and Hope, J., 2016, Early sponges and toxic protists: possible sources of cryostane, an age diagnostic biomarker antedating Sturtian Snowball Earth: *Geobiology*, v. 14, p. 129-149.
- Canfield, D. E., Poulton, S. W., Knoll, A. H., Narbonne, G. M., Ross, G., Goldberg, T., and Strauss, H., 2008, Ferruginous conditions dominated later neoproterozoic deep-water chemistry: *Science*, v. 321, p. 949-952.
- Cohen, A. S., Coe, A. L., Bartlett, J. M., and Hawkesworth, C. J., 1999, Precise Re–Os ages of organic-rich mudrocks and the Os isotope composition of Jurassic seawater: *Earth and Planetary Science Letters*, v. 167, no. 3, p. 159-173.
- Colodner, D., Sachs, J., Ravizza, G., Turekian, K., Edmond, J., and Boyle, E., 1993, The geochemical cycle of rhenium: a reconnaissance: *Earth and Planetary Science Letters*, v. 117, no. 1-2, p. 205-221.
- Condon, D.J., and Bowring, S.A., 2011, Chapter 9 A user's guide to Neoproterozoic geochronology: *Geological Society, London, Memoirs*, v. 36, p. 135–149.
- Corsetti, F.A., Extinction before the Snowball: *Nature Geoscience*, v. 2, p.386-387.
- Cox, G. M., Halverson, G. P., Stevenson, R. K., Vokaty, M., Poirier, A., Kunzmann, M., Li, Z.-X., Denyszyn, S. W., Strauss, J. V., and Macdonald, F. A., 2016, Continental flood basalt weathering as a trigger for Neoproterozoic Snowball Earth: *Earth and Planetary Science Letters*, v. 446, p. 89-99.
- Creaser, R., Papanastassiou, D., and Wasserburg, G., 1991, Negative thermal ion mass spectrometry of osmium, rhenium and iridium: *Geochimica et Cosmochimica Acta*, v. 55, p. 397-401.
- Creaser, R. A., Sannigrahi, P., Chacko, T., and Selby, D., 2002, Further evaluation of the Re-Os geochronometer in organic-rich sedimentary rocks: A test of hydrocarbon maturation effects in the Exshaw Formation, Western Canada Sedimentary Basin: *Geochimica et Cosmochimica Acta*, v. 66, p. 3441-3452.
- Crusius, J., and Thomson, J., 2000, Comparative behavior of authigenic Re, U, and Mo during reoxidation and subsequent long-term burial in marine sediments: *Geochimica et Cosmochimica Acta*, v. 64, no. 13, p. 2233-2242.
- Cumming, G. L., 1969, A recalculation of the age of the solar system, *Can. J. Earth Sci.*, v. 4, p. 719–735.
- Cumming, V.M., Poulton, S.W., Rooney, A.D., and Selby, D., 2013, Anoxia in the terrestrial environment during the Late Mesoproterozoic: *Geology*, v. 41, p. 583-586.
- Dahl, T. W., Canfield, D. E., Rosing, M. T., Frei, R. E., Gordon, G. W., Knoll, A. H., and Anbar, A. D., 2011, Molybdenum evidence for expansive sulfidic water masses in ~750 Ma oceans: *Earth and Planetary Science Letters*, v. 311, no. 3-4, p. 264-274.
- Dehler, C.M., Elrick, M., Karlstrom, K.E., Smith, G.A., Crossey, L.J., and Timmons, J.M., 2001, Neoproterozoic Chuar Group (~800–742 Ma), Grand Canyon: A record of cyclic marine deposition during global cooling and supercontinent rifting: *Sedimentary Geology*, v. 141–142, p. 465–499, doi:10.1016/S0037-0738(01)00087-2.

- Dehler, C.M., Elrick, M.E., Bloch, J.D., Karlstrom, K.E., Crossey, L.J., DesMarais, D., 2005. High-resolution $\delta^{13}\text{C}$ stratigraphy of the Chuar Group (~770-742 Ma), Grand Canyon: Implications for mid-Neoproterozoic climate change, *Geological Society of America Bulletin*, v. 117, p. 32-45
- Dehler, C.M., Porter, S.M., De Grey, L.D., Sprinkel, D.A., Brehm, A., 2007, The Neoproterozoic Uinta Mountain Group revisited: A synthesis of recent work on the Red Pine Shale and related undivided clastic strata, Northeastern Utah: in Link, P.K., and Lewis, R.S., eds., *Proterozoic Geology of western North America and Siberia*, Society of Sedimentary Geology Special Publication 86, p. 151-166
- Dehler, C.M., Fanning, C.M., Link, P.K., Kingsbury, E.M., and Rybczynski, D., 2010, Maximum depositional age and provenance of the Uinta Mountain Group and Big Cottonwood Formation, northern Utah: Paleogeography of rifting western Laurentia: *Geological Society of America Bulletin*, v. 122, p. 1686–1699, doi:10.1130/B30094.1.
- Dehler, C.M., Gehrels, G., Porter, S.M., Heizler, M., Karlstrom, K.E., Cox, G., Crossey, L., Timmons, M., 2017, Synthesis of the 780-740 Ma Chuar Group, Uinta Mountain Group, and Pahrump Group (ChUMP) strata, western U.S.: Implications for Laurentia-wide cratonic marine basins: *Geological Society of America Bulletin*, v. 129, p. 607-624
- Esser, B. K., and Turekian, K. K., 1993, The osmium isotopic composition of the continental crust: *Geochimica et Cosmochimica Acta*, v. 57, p. 3093-3104.
- Finlay, A.J., Selby, D., and Gröcke, D.R., 2010, Tracking the Hirnantian glaciation using Os isotopes: *Earth and Planetary Science Letters*, v. 293, p. 339-348.
- Ford, T.D., and Breed, W.J., 1973, Late Precambrian Chuar Group, Grand Canyon, Arizona: *Geological Society of America Bulletin*, v. 84, p. 1,243–1,260.
- Georgiev, S., Stein, H. J., Hannah, J. L., Bingen, B., Weiss, H. M., and Piasecki, S., 2011, Hot acidic Late Permian seas stifle life in record time: *Earth and Planetary Science Letters*, v. 310, p. 389-400.
- Georgiev, S., Stein, H. J., Hannah, J. L., Weiss, H. M., Bingen, B., Xu, G., Rein, E., Hatlø, V., Løseth, H., Nali, M., and Piasecki, S., 2012, Chemical signals for oxidative weathering predict Re–Os isochroneity in black shales, East Greenland: *Chemical Geology*, v. 324-325, p. 108-121.
- Halverson, G.P., Hoffman, P.F., Schrag, D.P., Maloof, A.C., and Rice A.H.N., 2005, Toward a Neoproterozoic composite carbon-isotope record: *Geological Society of America Bulletin* v.117, p.181-1207.
- Halverson, G. P., Wade, B. P., Hurtgen, M. T., and Barovich, K. M., 2010, Neoproterozoic chemostratigraphy: *Precambrian Research*, v. 182, p. 337–350.
- Hansen, W.R., 1965, *Geology of the Flaming Gorge Area, Utah-Colorado-Wyoming*: U.S. Geological Survey Professional Paper 490, 196 p.
- Hattori, Y., Suzuki, K., Honda, M., and Shimizu, H., 2003, Re-Os isotope systematics of the Taklimakan Desert sands, moraines and river sediments around the Taklimakan Desert, and of Tibetan soils: *Geochimica et Cosmochimica Acta*, v.67, p. 1203-1213.
- Horodyski, R.J., 1993, Paleontology of Proterozoic shales and mudstones: examples from the Belt Supergroup, Chuar Group and Pahrump Group, western USA: *Precambrian Research*, v. 61, p. 241-278
- Jaffe, L.A., Peucker-Ehrenbrink, B., and Petsch, S.T., 2002, Mobility of rhenium, platinum group elements and organic carbon during black shale weathering: *Earth and Planetary Science Letters*, v. 198, p. 339-353.

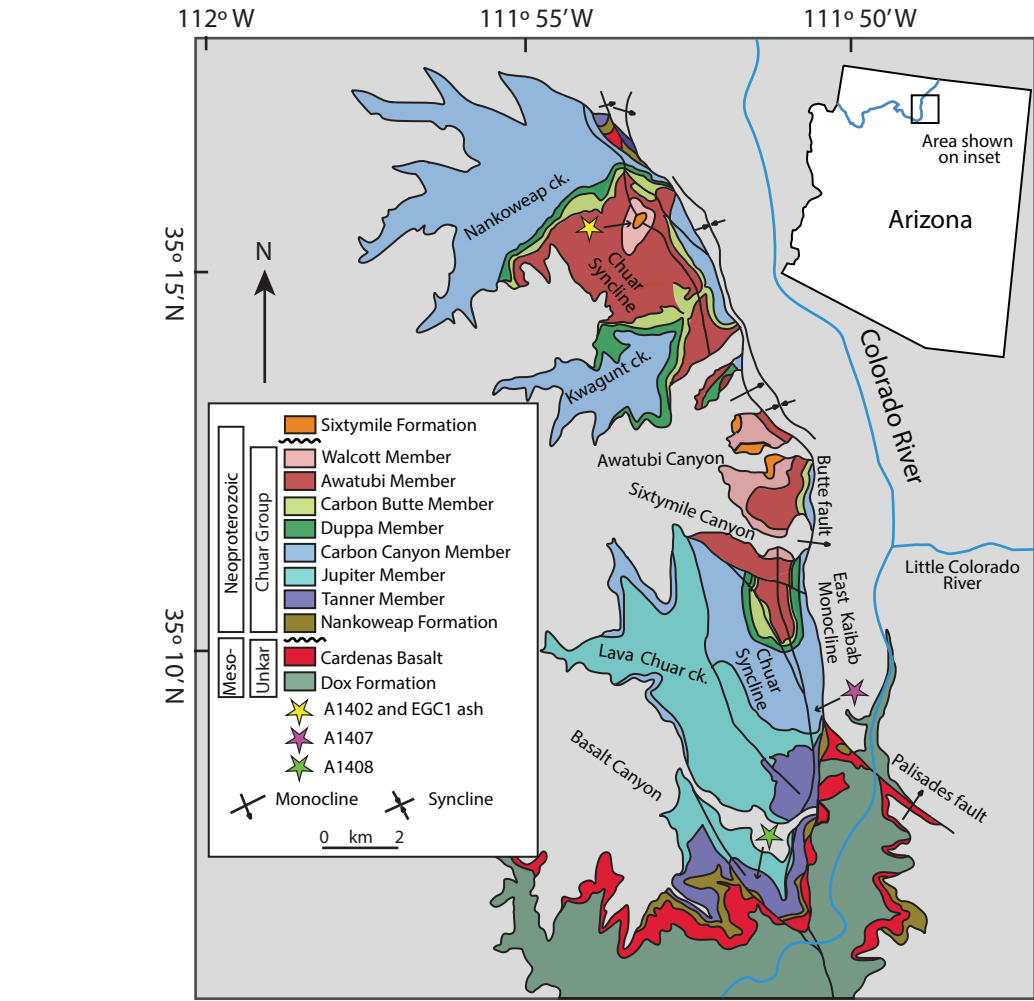
- Jaffey, A.H., Flynn, K.F., Glendenin, L.E., Bentley, W.T. and Essling, A.M., 1971, Precision measurement of half-lives and specific activities of U235 and U238. *Physical Review C*, v. 4, p.1889.
- Jefferson, C.W., and Parrish, R., 1989, Late Proterozoic stratigraphy, U/Pb zircon ages and rift tectonics, Mackenzie Mountains, northwestern Canada: *Canadian Journal of Earth Sciences*, v. 26, p. 1784–1801, doi:10.1139/e89-151.
- Johnston, D. T., Poulton, S. W., Dehler, C., Porter, S., Husson, J., Canfield, D. E., and Knoll, A. H., 2010, An emerging picture of Neoproterozoic ocean chemistry: Insights from the Chuar Group, Grand Canyon, USA: *Earth and Planetary Science Letters*, v. 290, no. 1-2, p. 64-73.
- Karlstrom, K.E., Bowring, S.A., Dehler, C.M., Knoll, A.H., Porter, S.M., Des Marais, D.J., Weil, A.B., Sharp, Z.D., Geissman, J.W., Elrick, M.B., Timmons, J.M., Crossey, L.J., and Davidek, K.L., 2000, Chuar Group of the Grand Canyon: record of breakup of Rodinia, associated change in the global carbon cycle, and ecosystem expansion by 740 Ma: *Geology*, v. 28, p. 619–622.
- Kendall B. S., Creaser R. A., Ross G. M. and Selby D., 2004, Constraints on the timing of Marinoan “Snowball Earth” glaciation by ^{187}Re – ^{187}Os dating of a Neoproterozoic, post-glacial black shale in Western Canada: *Earth and Planetary Science Letters*, v. 222, p. 729–740
- Kendall, B., Creaser, R. A., and Selby, D., 2006, Re–Os geochronology of postglacial black shales in Australia: Constraints on the timing of “Sturtian” glaciation: *Geology*, v. 34, no. 9, p. 729-732.
- Kendall, B., Creaser, R. A., and Selby, D., 2009a, ^{187}Re – ^{187}Os geochronology of Precambrian organic-rich sedimentary rocks: *Geological Society, London, Special Publications*, v. 326, p. 85-107.
- Kendall, B., Creaser, R. A., Gordon, G. W., and Anbar, A. D., 2009b, Re–Os and Mo isotope systematics of black shales from the Middle Proterozoic Velkerri and Wollgorang Formations, McArthur Basin, northern Australia: *Geochimica et Cosmochimica Acta*, v. 73, no. 9, p. 2534-2558.
- Knoll, A. H., Javaux, E. J., Hewitt, D., and Cohen, P., 2006, Eukaryotic organisms in Proterozoic oceans: *Philosophical Transactions of the Royal Society B: Biological Sciences*, v. 361, p. 1023–1038.
- Knoll, A.H., 2014, Paleobiological perspectives on early eukaryotic evolution: *Cold Spring Harbor Perspectives in Biology*, v. 6, 14 p., <http://ddx.doi.org10.1101/cshperspect.a016121>.
- Ludwig, K.R., 1980, Calculation of uncertainties of U–Pb isotope data: *Earth and Planetary Science Letters* v. 46, p.212–220
- Ludwig, K., 2009, Isoplot 4.1. A geochronological toolkit for Microsoft Excel: Berkeley Geochronology Center Special Publication, v. 4, p. 76.
- Ludwig, K. R., 2003, User's manual for Isoplot 3.00: a geochronological toolkit for Microsoft Excel, Kenneth R. Ludwig, v. 4.
- Levasseur, S., Birck, J. L. and Allègre, C. J., 1998, Direct measurement of femtomoles of osmium and the $^{187}\text{Os}/^{186}\text{Os}$ ratio in seawater: *Science*, v. 282, p. 272-274.
- Li, Z-X., Evans, D.A.D., and Halverson, G.P., 2013, Neoproterozoic glaciations in a revised global palaeogeography from the breakup of Rodinia to the assembly of Gondwanaland: *Sedimentary Geology*, v. 294, p. 219-232.

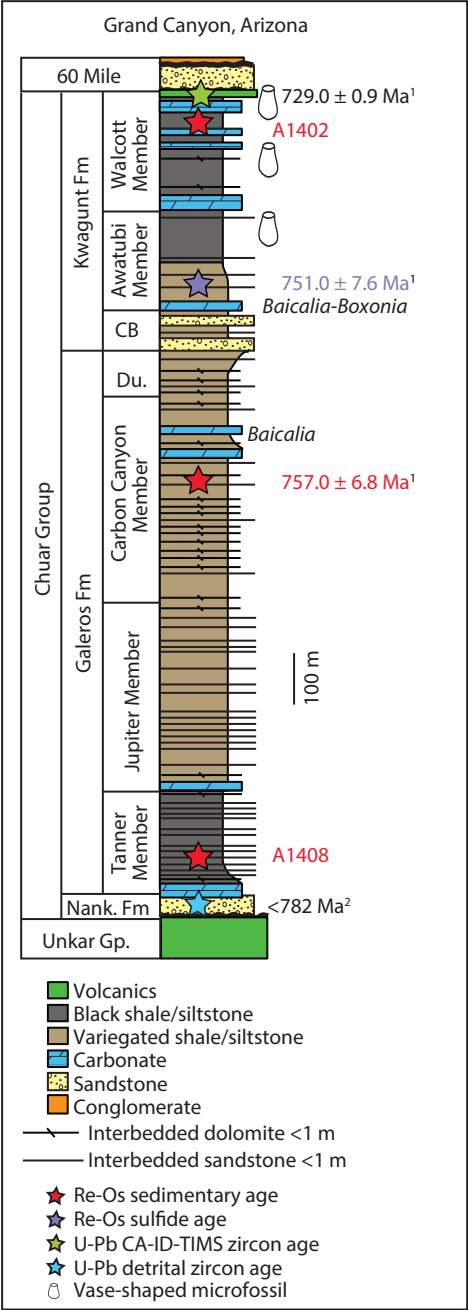
- Lillis, P.G., 2016, The Chuar petroleum system, Arizona and Utah, *in* Dolan, M.P., Higley, D.K., Lillis, P.G., eds., Hydrocarbon source rocks in unconventional plays, Rocky Mountain Region: Rocky Mountain Association of Geologists, Chapter 3 p. 79-137.
- Macdonald, F. A., Schmitz, M. D., Crowley, J. L., Roots, C. F., Jones, D. S., Maloof, A. C., Strauss, J. V., Cohen, P. A., Johnston, D. T., and Schrag, D. P., 2010, Calibrating the Cryogenian: *Science*, v. 327, p. 1241–1243.
- Macdonald, F. A., Prave, A. R., Petterson, R., Smith, E. F., Pruss, S. B., Oates, K., Waechter, F., Trotsuk, D., and Fallick, A. E., 2013, The Laurentian record of Neoproterozoic glaciation, tectonism, and eukaryotic evolution in Death Valley, California: *Geological Society of America Bulletin*, v. 125, no. 7-8, p. 1203-1223.
- Mahon, R.C., Dehler, C.M., Link, P.K., Karlstrom, K.E., and Gehrels, G.E., 2014, Geochronologic and stratigraphic constraints on the Mesoproterozoic and Neoproterozoic Pahrump Group, Death Valley, California: A record of the assembly, stability, and break of Rodinia: *Geological Society of America Bulletin*, v. 126, p. 652–664, <http://dx.doi.org/10.1130/B30956.1>.
- McDougall I., and Harrison, T.M., 1999, Appendix 4 A.1 Isochron Analysis, *in* McDougall I., and Harrison, T.M., 1999, *Geochronology and Thermochronology by the ³⁹Ar/⁴⁰Ar Method*, Oxford University Press, New York, p. 134-136.
- Morelli, R.M., Creaser, R.A., Selby, D., Kontak, D.J., and Horne, R.J., 2005, Rhenium-Osmium of Arsenopyrite in Meguma Group gold deposits, Meguma Terrane, Nova Scotia, Canada: Evidence of multiple gold-mineralizing events: *Economic Geology*, v. 100, p. 1229-1241.
- Nagy, R. M., Porter, S. M., Dehler, C. M., and Shen, Y., 2009, Biotic turnover driven by eutrophication before the Sturtian low-latitude glaciation: *Nature Geoscience*, v. 2, p. 415-418.
- Narbonne, G.M., Kaufman, A.J., and Knoll, A.H., 1994, Integrated chemostratigraphy and biostratigraphy of the Windermere Supergroup, northwestern Canada: Implications for Neoproterozoic correlations and the early evolution of animals: *Geological Society of America Bulletin*, v. 106, p. 1281–1292, [http://dx.doi.org/10.1130/0016-7606\(1994\)106/1281:ICABOT/2.3.CO;2](http://dx.doi.org/10.1130/0016-7606(1994)106/1281:ICABOT/2.3.CO;2).
- Olsen, P. E., 1990, Tectonic, climatic, and biotic modulation of lacustrine ecosystems—examples from Newark Supergroup of eastern North America: *Lacustrine basin exploration: Case studies and modern analogs: AAPG Memoir*, v. 50, p. 209-224.
- Peucker-Ehrenbrink, B., and Hannigan, R. E., 2000, Effects of black shale weathering on the mobility of rhenium and platinum group elements: *Geology*, v. 28, no. 5, p. 475-478.
- Peucker- Ehrenbrink, B., and Ravizza, G., 2000, The marine osmium isotope record: *Terra Nova*, v. 12, p. 205-219.
- Peucker- Ehrenbrink, B., and Jahn, B. m., 2001, Rhenium- osmium isotope systematics and platinum group element concentrations: Loess and the upper continental crust: *Geochemistry, Geophysics, Geosystems*, v. 2, no. 10.
- Pierson-Wickmann, A.-C., Reisberg, L., and France-Lanord, C., 2002, Behavior of Re and Os during low-temperature alteration: results from Himalayan soils and altered black shales: *Geochimica et Cosmochimica Acta*, v. 66, no. 9, p. 1539-1548.
- Planavsky, N. J., Reinhard, C. T., Wang, X., Thomson, D., McGoldrick, P., Rainbird, R. H., Johnson, T., Fischer, W. W., and Lyons, T. W., 2014, Earth history. Low mid-Proterozoic atmospheric oxygen levels and the delayed rise of animals: *Science*, v. 346, p. 635-638.

- Poirier, A., and Hillaire- Marcel, C., 2011, Improved Os- isotope stratigraphy of the Arctic Ocean: *Geophysical Research Letters*, v. 38, no. 14.
- Porter, S., 2011, The rise of predators: *Geology*, v. 39, no. 6, p. 607-608.
- Porter, S.M., and Riedman, L.A., 2016, Systematics of organic-walled microfossils from the ca. 780–740 Ma Chuar Group, Grand Canyon, Arizona: *Journal of Paleontology*, v. 90, no. 5, p. 815-853.
- Porter, S.M., and Knoll, A.H., 2000, Testate amoebae in the Neoproterozoic Era: evidence from vase-shaped microfossils in the Chuar Group, Grand Canyon: *Paleobiology*, v. 26, p. 360–385, [http://dx.doi.org/10.1666/0094-8373\(2000\)026_0360:TAITNE_2.0.CO;2](http://dx.doi.org/10.1666/0094-8373(2000)026_0360:TAITNE_2.0.CO;2)
- Porter, S.M., Meisterfeld, R., and Knoll, A.H., 2003, Vase-shaped microfossils from the Neoproterozoic Chuar Group, Grand Canyon: A classification guided by modern testate amoebae: *Journal of Paleontology*, v. 77, p. 409–429, [http://dx.doi.org/10.1666/0022-3360\(2003\)077/0409:VMFTNC/2.0.CO;2](http://dx.doi.org/10.1666/0022-3360(2003)077/0409:VMFTNC/2.0.CO;2).
- Ravizza, G., and Turekian, K., 1992, The osmium isotopic composition of organic-rich marine sediments: *Earth and Planetary Science Letters*, v. 110, p. 1-6.
- Ravizza, G., Turekian, K., and Hay, B., 1991, The geochemistry of rhenium and osmium in recent sediments from the Black Sea: *Geochimica et Cosmochimica Acta*, v. 55, no. 12, p. 3741-3752.
- Ravizza, G., and Turekian, K. K., 1989, Application of the ^{187}Re - ^{187}Os system to black shale geochronometry: *Geochimica et Cosmochimica Acta*, v. 53, p. 3257-3262.
- Riedman, L. A., and Porter, S., 2016, Organic-walled microfossils of the mid-Neoproterozoic Alinya Formation, Officer Basin, Australia: *Journal of Paleontology*, v. 90, no. 5, p. 854-887.
- Rivera, T.A., Schmitz, M.D., Jicha, B.R., and Crowley, J.L., 2016, Zircon petrochronology and $^{40}\text{Ar}/^{39}\text{Ar}$ sanidine dates for the Mesa Falls Tuff: Crystal-scale records of magmatic evolution and the short lifespan of a large Yellowstone magma chamber: *Journal of Petrology*, doi: 10.1093/petrology/egw053.
- Rivera, T.A., Storey, M., Schmitz, M.D., and Crowley, J.L., 2013, Age intercalibration of $^{40}\text{Ar}/^{39}\text{Ar}$ sanidine and chemically distinct U/Pb zircon populations from the Alder Creek Rhyolite Quaternary geochronology standard: *Chemical Geology*, v. 345, p. 87–98.
- Rooney, A.D., Selby, D., Houzay, J.-P. and Renne, P.R., 2010, Re-Os geochronology of a Mesoproterozoic sedimentary succession, Taoudeni basin, Mauritania: Implications for basin-wide correlations and Re-Os organic-rich sediments systematics: *Earth and Planetary Science Letters*, v. 289, p. 486-496.
- Rooney, A. D., Macdonald, F. A., Strauss, J. V., Dudas, F. Ö., Hallmann, C., and Selby, D., 2014, Re-Os geochronology and coupled Os-Sr isotope constraints on the Sturtian snowball Earth: *Proceedings of the National Academy of Sciences of the United States of America*, v. 111, p. 51–56, <http://dx.doi.org/10.1073/pnas.1317266110>
- Rooney, A. D., Strauss, J. V., Brandon, A. D., and Macdonald, F. A., 2015, A Cryogenian chronology: Two long-lasting, synchronous Neoproterozoic glaciations: *Geology*, v. 43, p. 459–462, <http://dx.doi.org/10.1130/G36511.1>
- Rooney, A. D., Chew, D. M., and Selby, D., 2011, Re–Os geochronology of the Neoproterozoic–Cambrian Dalradian Supergroup of Scotland and Ireland: Implications for Neoproterozoic stratigraphy, glaciations and Re–Os systematics: *Precambrian Research*, v. 185, no. 3-4, p. 202-214.

- Schaefer, B. F., and Burgess, J. M., 2003, Re-Os isotopic age constraints on deposition in the Neoproterozoic Amadeus Basin: implications for the 'Snowball Earth': *Journal of the Geological Society*, v. 160, no. 6, p. 825-828.
- Schmitz, M.D., and Schoene B., 2007, Derivation of isotope ratios, errors, and error correlations for U–Pb geochronology using ^{205}Pb – ^{235}U –(^{233}U)-spiked isotope dilution thermal ionization mass spectrometric data. *Geochemistry, Geophysics, Geosystems* 8: Q08006.
- Schmitz, M.D., 2012, Radiogenic Isotope Geochronology, *in* Gradstein, F.M., Ogg, J.G., Schmitz, M.D., and Ogg, G.M. eds., *The Geologic Time Scale 2012*, Amsterdam, Elsevier, p. 115–126.
- Schoonen, M., and Barnes, H., 1991, Reactions forming pyrite and marcasite from solution: II. Via FeS precursors below 100 C: *Geochimica et Cosmochimica Acta*, v. 55, p. 1505-1514.
- Schoonen, M. A., 2004, Mechanisms of sedimentary pyrite formation: *Geological Society of America Special Papers*, v. 379, p. 117-134.
- Selby, D., Mutterlose, J., and Condon, D. J., 2009, U–Pb and Re–Os geochronology of the Aptian/Albian and Cenomanian/Turonian stage boundaries: Implications for timescale calibration, osmium isotope seawater composition and Re–Os systematics in organic-rich sediments: *Chemical Geology*, v. 265, no. 3-4, p. 394-409.
- Selby, D., 2007, Direct Rhenium-Osmium age of the Oxfordian-Kimmeridgian boundary, Staffin bay, Isle of Skye, UK, and the Late Jurassic time scale: *Norsk Geologisk Tidsskrift*, v. 87, p. 291.
- Selby, D., and Creaser, R. A., 2003, Re–Os geochronology of organic rich sediments: an evaluation of organic matter analysis methods: *Chemical Geology*, v. 200, p. 225-240.
- Selby, D., and Creaser, R. A., 2005, Direct radiometric dating of the Devonian-Mississippian time-scale boundary using the Re-Os black shale geochronometer: *Geology*, v. 33, p. 545.
- Sharma, M., Papanastassiou, D., and Wasserburg, G., 1997, The concentration and isotopic composition of osmium in the oceans: *Geochimica et Cosmochimica Acta*, v. 61, p. 3287-3299.
- Shields-Zhou, G. A., Porter, S., and Halverson, G. P. 2016, A New Rock-Based Definition for the Cryogenian Period (Circa 720-635 Ma): *Episodes*, v. 39, p. 3-8.
- Smith, E. F., MacDonald, F. A., Crowley, J. L., Hodgins, E. B., and Schrag, D. P., 2016, Tectonostratigraphic evolution of the c. 780–730 Ma Beck Spring Dolomite: Basin Formation in the core of Rodinia: *Geological Society, London, Special Publications*, v. 424, p. 213-239.
- Smoliar, M.I., Walker, R.J., and Morgan, J.W., 1996, Re-Os isotope constraints on the age of Group IIA, IIIA, IVA, and IVB iron meteorites: *Science*, v. 271, p. 1099-1102.
- Spence, G. H., Le Heron, D. P., and Fairchild, I. J., 2016, Sedimentological perspectives on climatic, atmospheric and environmental change in the Neoproterozoic Era: *Sedimentology*, v. 63, no. 2, p. 253-306.
- Stacey, J.C., and Kramers, J.D., 1975, Approximation of terrestrial lead isotope evolution by a two-stage model: *Earth and Planetary Science Letters* v. 26 p. 207–221.
- Strauss, J. V., Rooney, A. D., Macdonald, F. A., Brandon, A. D., and Knoll, A. H., 2014, 740 Ma vase-shaped microfossils from Yukon, Canada: Implications for Neoproterozoic chronology and biostratigraphy: *Geology*, v. 42, p. 659–662, <http://dx.doi.org/10.1130/G35736.1>

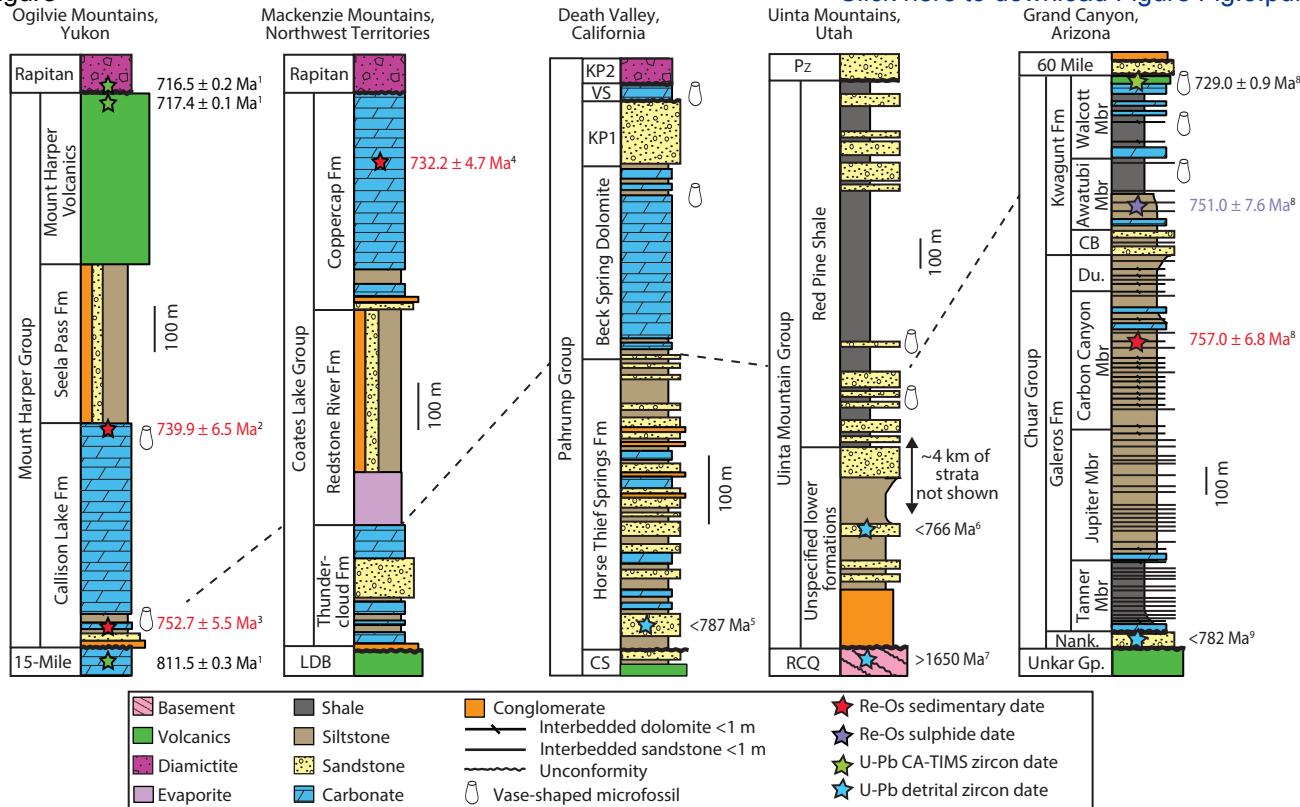
923 Strauss, J.V., Macdonald, F.A., Halverson, G.P., Tosca, N.J., Schrag, D.P. and Knoll, A.H.,
 924 2015, Stratigraphic evolution of the Neoproterozoic Callison Lake Formation: Linking
 925 the break-up of Rodinia to the Islay carbon isotope excursion: *American Journal of*
 926 *Science*, v. 315, p.881-944
 927 Summons, R. E., Brassell, S. C., Eglinton, G., Evans, E., Horodyski, R. J., Robinson, N., and
 928 Ward, D. M., 1988, Distinctive hydrocarbon biomarkers from fossiliferous sediment of
 929 the Late Proterozoic Walcott Member, Chuar Group, Grand Canyon, Arizona:
 930 *Geochimica et Cosmochimica Acta*, v. 52, p. 2625-2637.
 931 Sun, W., Bennett, V. C., Eggins, S. M., Kamenetsky, V. S., and Arculus, R. J., 2003, Enhanced
 932 mantle-to-crust rhenium transfer in undegassed arc magmas: *Nature*, v. 422, p. 294-297.
 933 Timmons, J.M., Karlstrom, K.E., Dehler, C.M., Geissman, J.W., and Heizler, M.T., 2001,
 934 Proterozoic multistage (ca. 1.1. and 0.8 Ga) extension in the Grand Canyon Supergroup
 935 and establishment of a northwest- and northtrending tectonic grain in the southwestern
 936 United States: *Geological Society of America Bulletin*, v. 113, p. 163–181,
 937 [http://dx.doi.org/10.1130/0016-7606\(2001\)113/0163:PMCAGE/2.0.CO;2](http://dx.doi.org/10.1130/0016-7606(2001)113/0163:PMCAGE/2.0.CO;2).
 938 Völkening, J., Walczyk, T., and Heumann, K. G., 1991, Osmium isotope ratio determinations by
 939 negative thermal ionization mass spectrometry: *International Journal of Mass*
 940 *Spectrometry and Ion Processes*, v. 105, no. 2, p. 147-159.
 941 Wendt, I. and Carl, C., 1991, The statistical distribution of the mean squared weighted deviation.
 942 *Chemical Geology: Isotope Geoscience Section*, v. 86, p. 275-285.
 943 Woodhouse, O., Ravizza, G., Falkner, K. K., Statham, P., and Peucker-Ehrenbrink, B., 1999,
 944 Osmium in seawater: vertical profiles of concentration and isotopic composition in the
 945 eastern Pacific Ocean: *Earth and Planetary Science Letters*, v. 173, p. 223-233.
 946 Xu, W., Ruhl, M., Jenkyns, H. C., Hesselbo, S. P., Riding, J. B., Selby, D., Naafs, B. D. A.,
 947 Weijers, J. W. H., Pancost, R. D., Tegelaar, E. W., and Idiz, E. F., 2017, Carbon
 948 sequestration in an expanded lake system during the Toarcian oceanic anoxic event:
 949 *Nature Geoscience* v. 10, p. 129-134.
 950 York, D., 1969, Least squares fitting of a straight line with correlated errors. *Earth and Planetary*
 951 *Science Letters*, v. 5, p. 320-324.
 952 York, D., Evensen, N., Martinez, M., and Delgado J., 2004. Unified equations for the slope,
 953 intercept, and standard errors of the best straight line, *Am. J. Phys.* v. 72 p. 367-375.
 954 Yang, G., Hannah, J. L., Zimmerman, A., Stein, H. J., and Bekker, A., 2009, Re–Os depositional
 955 age for Archean carbonaceous slates from the southwestern Superior Province:
 956 *Challenges and insights: Earth and Planetary Science Letters*, v. 280, no. 1-4, p. 83-92.
 957 Zheng, Y.-F., 1989, Influences of the nature of the initial RbSr system on isochron validity:
 958 *Chemical Geology: Isotope Geoscience section*, v. 80, no. 1, p. 1-16.

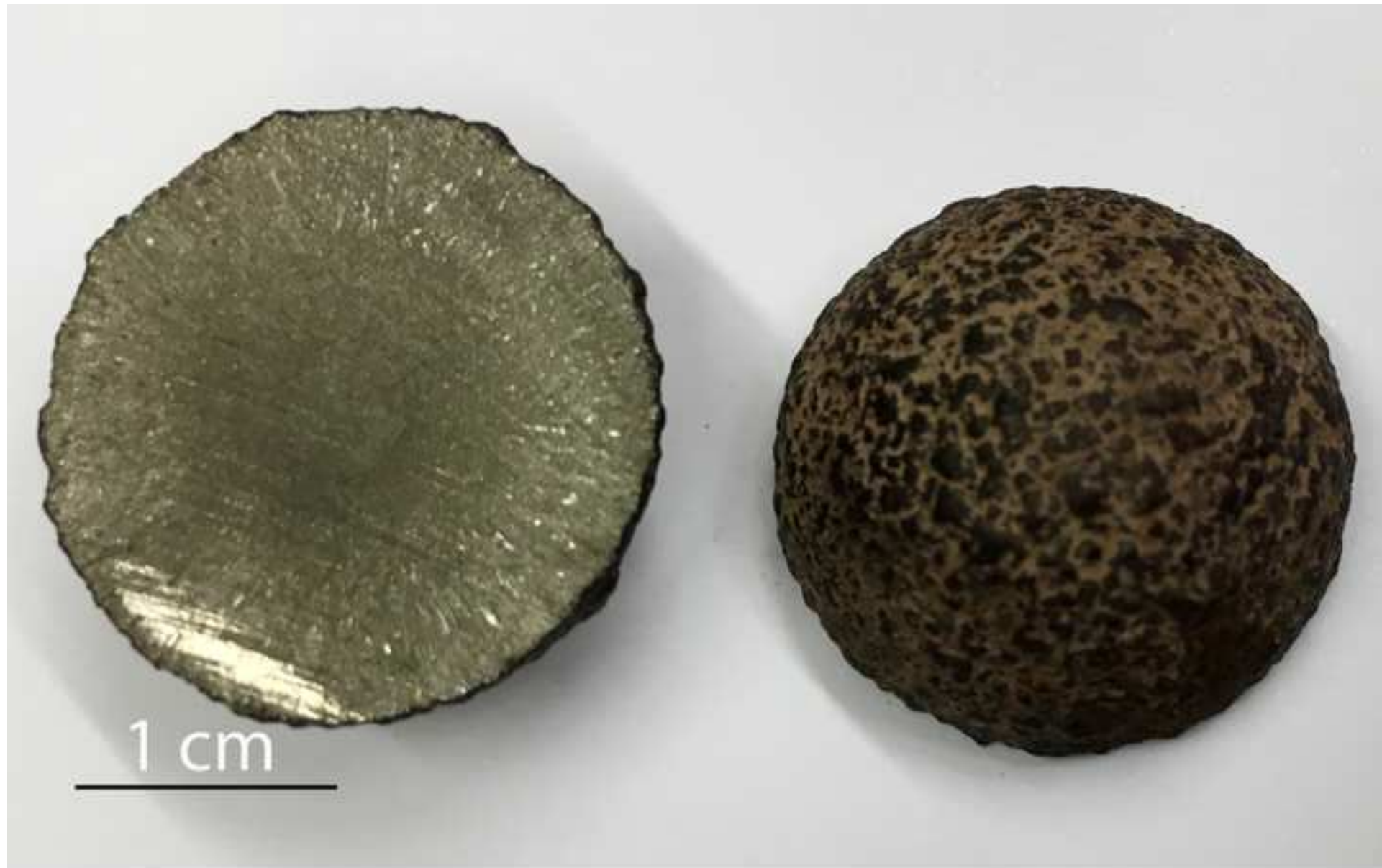


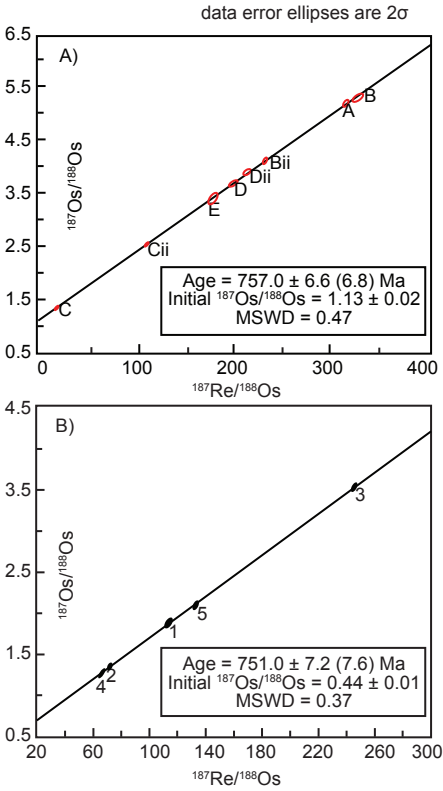


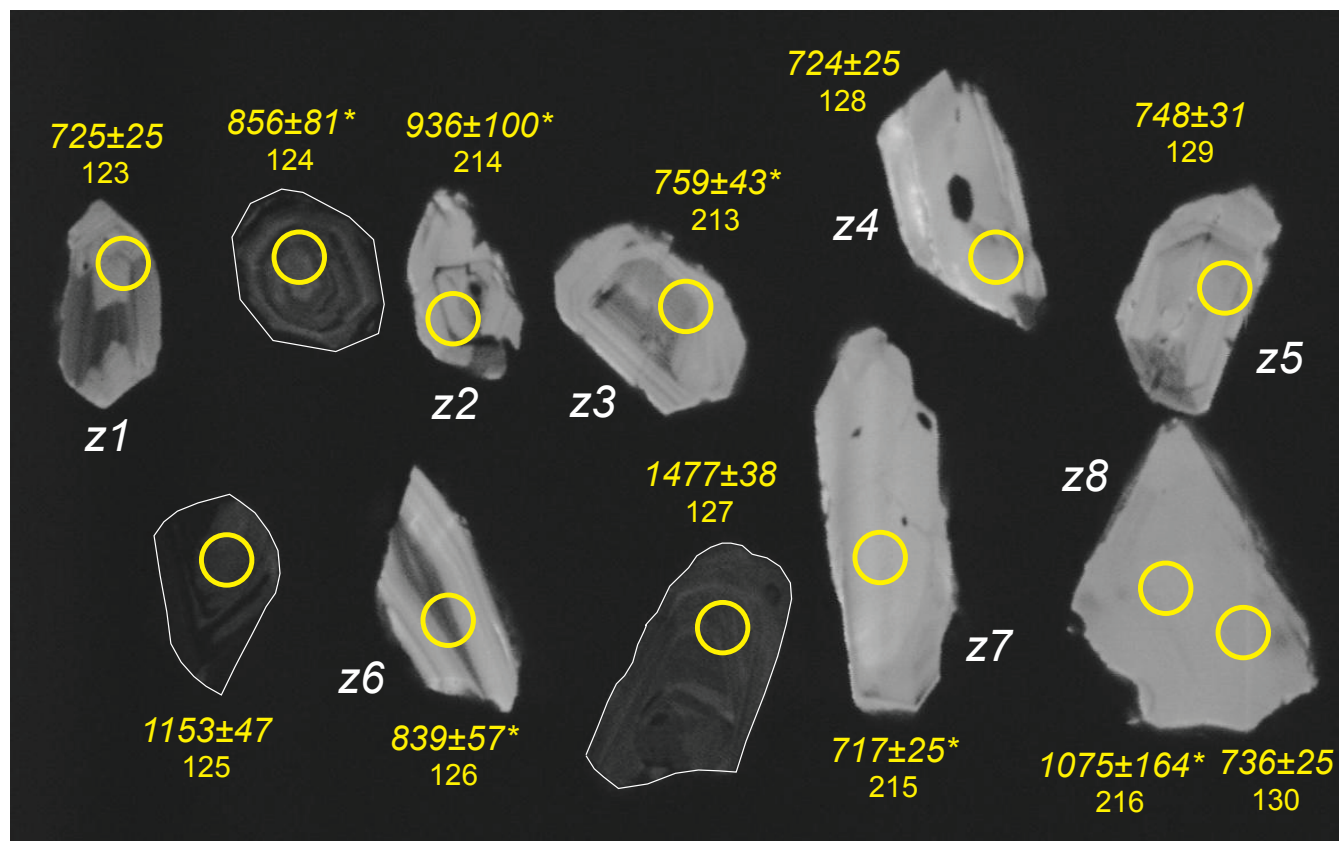
Figure

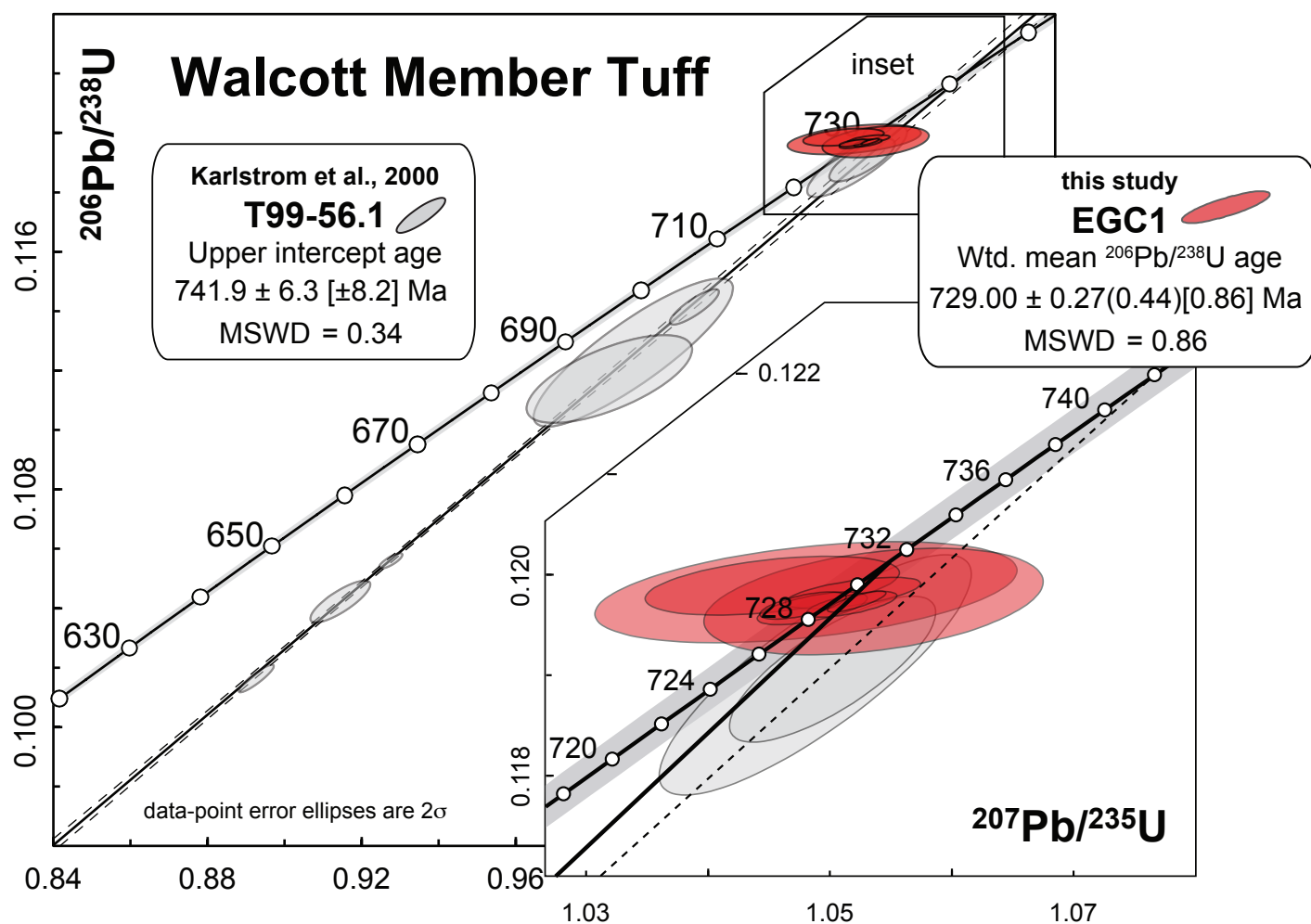
[Click here to download Figure Fig.3.pdf](#)

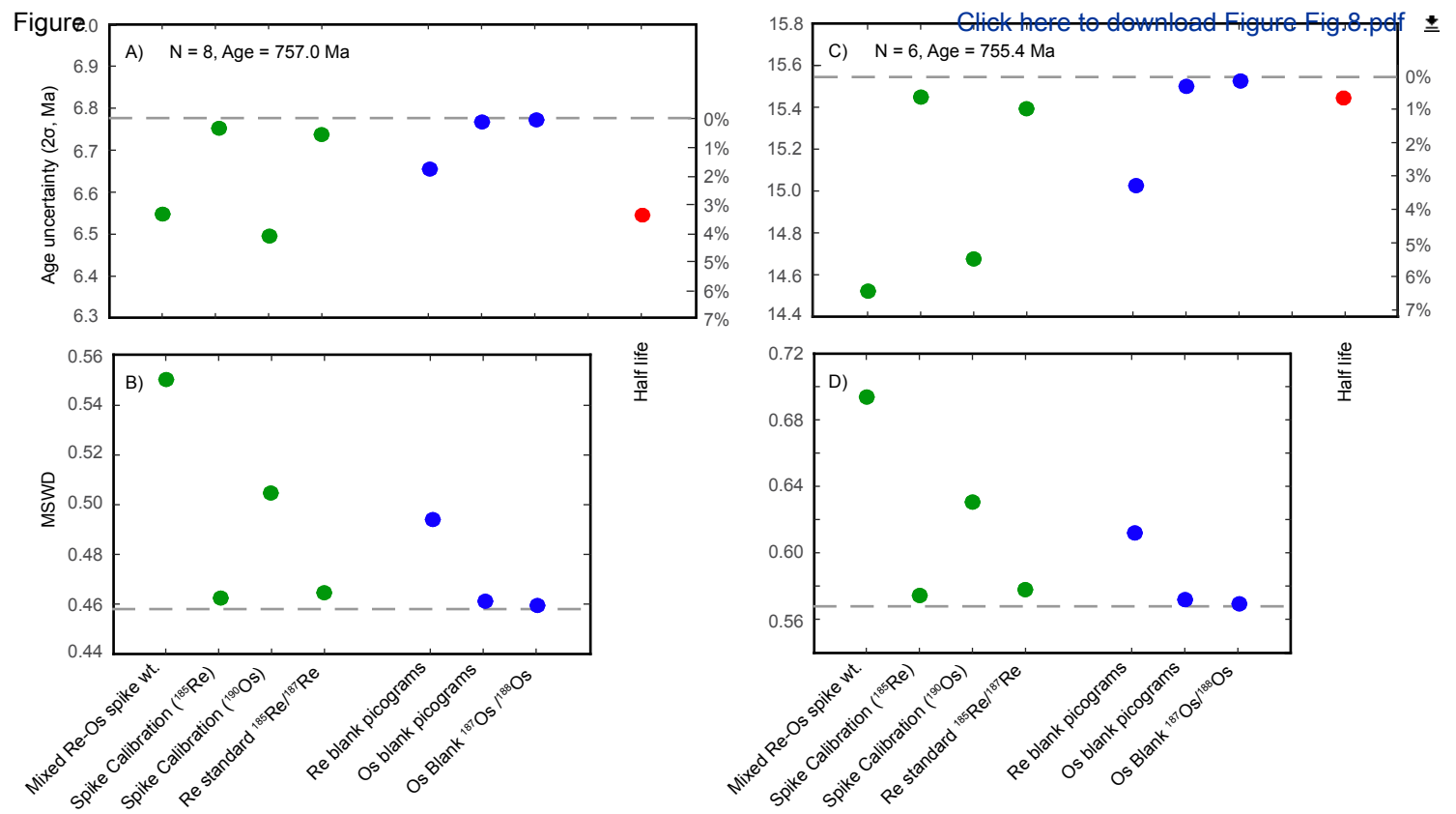












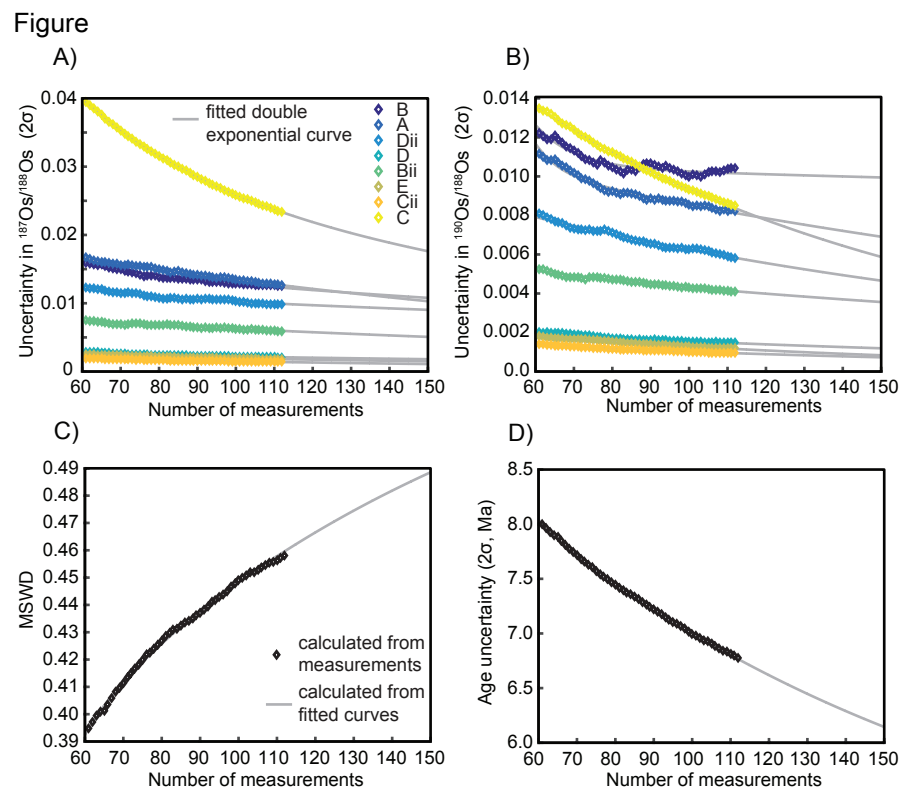


Table 1: Total Organic Carbon (TOC) and carbonate content of a selection of samples from A1402, 1407 & 1408. See text for discussion

	Sample	Carbonate content (wt. %)	Total Organic Carbon (wt. %)
A1402 Walcott member	A	80.37	0.82
	B	85.14	0.48
	Cii	77.18	0.72
	Dii	86.48	0.38
	E	77.42	0.66
	Average	81.32	0.61
A1407 Carbon Canyon member	A	89.30	0.11
	B	90.30	0.10
	C	89.80	0.11
	Average	89.80	0.11
A1408 Tanner member	F	81.16	0.50
	G	75.41	0.68
	H	81.38	0.46
	Average	79.32	0.55

Table 2. CA-IDTIMS U-Pb Isotopic Data

Table 2. CA-IDTIMS U-Pb Isotopic Data										Radiogenic Isotopic Ratios					Radiogenic Isotopic Dates					
Grain	$\frac{\text{Th}}{\text{U}}$	$^{206}\text{Pb}^*$ x10 ⁻¹³ mol	mol % $^{206}\text{Pb}^*$	$\frac{\text{Pb}^*}{\text{Pbc}}$	Pbc (pg)	$\frac{^{206}\text{Pb}}{^{204}\text{Pb}}$	$\frac{^{208}\text{Pb}}{^{206}\text{Pb}}$	$\frac{^{207}\text{Pb}}{^{206}\text{Pb}}$	% err	$\frac{^{207}\text{Pb}}{^{235}\text{U}}$	% err	$\frac{^{206}\text{Pb}}{^{238}\text{U}}$	% err	rho	$\frac{^{207}\text{Pb}}{^{206}\text{Pb}}$	±	$\frac{^{207}\text{Pb}}{^{235}\text{U}}$	±	$\frac{^{206}\text{Pb}}{^{238}\text{U}}$	±
(a)	(b)	(c)	(c)	(c)	(c)	(d)	(e)	(e)	(f)	(e)	(f)	(e)	(f)		(g)	(f)	(g)	(f)	(g)	(f)
EGC1 — Walcott Member Tuff																				
z1(123)	0.472	0.4718	95.07%	5.7	2.05	358	0.146	0.06366	0.38	1.05162	0.435	0.11982	0.104	0.607	730.2	8.1	729.69	2.26	729.51	0.72
z2(214)	0.513	0.1317	85.49%	1.8	1.88	122	0.158	0.06342	1.25	1.04775	1.362	0.11982	0.339	0.430	722.3	26.6	727.77	7.07	729.54	2.3
z3(213)	0.501	0.2313	81.93%	1.4	4.30	97	0.155	0.06380	1.01	1.05332	1.088	0.11973	0.358	0.375	735.1	21.4	730.52	5.67	729.03	2.5
z4(128)	0.498	0.3278	98.52%	20	0.41	1222	0.154	0.06354	0.30	1.04824	0.354	0.11966	0.110	0.627	726.2	6.3	728.01	1.84	728.60	0.76
z5(129)	0.467	0.4457	98.97%	29	0.38	1754	0.144	0.06348	0.23	1.04751	0.278	0.11969	0.090	0.648	724.2	4.9	727.65	1.45	728.76	0.62
z6(126)	0.575	0.2414	88.26%	2.3	2.70	150	0.178	0.06321	0.76	1.04494	0.822	0.11989	0.198	0.443	715.4	16.1	726.37	4.27	729.93	1.4
z7(215)	0.459	0.9841	99.11%	33	0.74	2013	0.142	0.06372	0.14	1.05193	0.189	0.11973	0.073	0.805	732.4	2.9	729.84	0.99	729.02	0.50
z8(216)	0.409	0.4896	98.32%	17.0	0.70	1065	0.126	0.06371	0.24	1.05149	0.291	0.11970	0.088	0.671	732.0	5.1	729.62	1.51	728.86	0.61

Notes:

(a) z1, z2, etc. are labels for single zircon grain fragments; associated LA-ICPMS spot analysis on same grain given in parentheses.

(b) Model Th/U ratio calculated from radiogenic $^{206}\text{Pb}/^{206}\text{Pb}$ ratio and $^{207}\text{Pb}/^{235}\text{U}$ date.

(c) Pb* and Pbc are radiogenic and common Pb, respectively. mol % $^{206}\text{Pb}^*$ is with respect to radiogenic and blank Pb.

(d) Measured ratio corrected for spike and fractionation only. Samples were spiked with the ET535 tracer, with internal double spike U fractionation correction, and external Pb fractionation correction of 0.16 ± 0.02 (1-sigma) %/amu (atomic mass unit), based on analysis of NBS-981 and NBS-982.

(e) Corrected for fractionation, spike, common Pb, and initial disequilibrium in $^{230}\text{Th}/^{238}\text{U}$. Up to 0.5 pg of common Pb assigned to procedural blank with composition of $^{206}\text{Pb}/^{204}\text{Pb} = 18.042 \pm 0.61\%$; $^{207}\text{Pb}/^{204}\text{Pb} = 15.537 \pm 0.52\%$; $^{208}\text{Pb}/^{204}\text{Pb} = 37.686 \pm 0.63\%$ (1-sigma). Excess over blank was assigned to initial common Pb, using the Stacey and Kramers (1975) two-stage Pb isotope evolution model at 729 Ma.

(f) Errors are 2-sigma, propagated using algorithms of Schmitz and Schoene (2007).

(g) Calculations based on the decay constants of Jaffey et al. (1971). $^{206}\text{Pb}/^{238}\text{U}$ and $^{207}\text{Pb}/^{206}\text{Pb}$ ratios and dates corrected for initial disequilibrium in $^{230}\text{Th}/^{238}\text{U}$ using a mineral-melt partition coefficient ratio for $D_{\text{Th/U}} = 0.2$.

Table 3: Re and Os elemental and isotopic data for samples A1407, 1402 and 1408. See text for discussion.

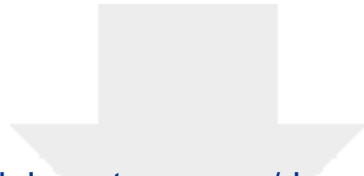
	Sample	Re (ng/g)	±	Os (pg/g)	±	¹⁸² Os (pg/g)	±	¹⁸⁷ Re/ ¹⁸⁸ Os	±	¹⁸⁷ Os/ ¹⁸⁸ Os	±	rho ^a	Osi at time ^b	Latitude	Longitude
A1407 Carbon Canyon member	A	2.83	0.01	71.61	0.54	17.89	0.09	314.43	1.87	5.128	0.036	0.589	757 Ma	36.1508	-111.833778
	B	1.93	0.01	47.66	0.44	11.82	0.10	324.28	3.19	5.226	0.053	0.648	1.14		
	Bii	2.88	0.01	91.12	0.67	24.90	0.13	230.04	1.45	4.043	0.030	0.606	1.11		
	C	0.45	0.01	151.32	1.33	53.98	0.41	16.52	0.25	1.333	0.027	0.183	1.13		
	Cii	1.73	0.01	91.23	0.57	28.25	0.14	121.96	0.82	2.681	0.019	0.537	1.12		
	D	1.35	0.01	46.53	0.39	13.04	0.10	205.71	1.89	3.753	0.038	0.606	1.15		
	Dii	1.82	0.01	61.08	0.46	16.99	0.10	213.55	1.56	3.841	0.032	0.566	1.13		
	E	1.15	0.01	42.98	0.46	12.37	0.14	184.32	2.36	3.459	0.053	0.637	1.12		
Marcasite nodules	1	3.59	0.01	186.72	2.05	62.71	0.90	113.90	1.68	1.885	0.041	0.651	751 Ma	36.28726	-111.888634
	2	3.09	0.02	239.41	1.50	85.26	0.61	72.13	0.65	1.348	0.014	0.812	0.45		
	3	13.47	0.03	382.12	2.71	109.30	1.20	245.21	1.46	3.528	0.027	0.642	0.44		
	4	3.46	0.02	289.31	2.86	103.95	1.50	66.14	1.00	1.270	0.028	0.814	0.44		
	5	3.54	0.01	161.73	1.37	53.10	1.00	132.67	1.33	2.103	0.029	0.666	0.44		
A1402 Walcott member	A	21.12	0.06	237.68	1.75	64.10	0.18	653.02	3.89	4.154	0.031	0.636	740 Ma	36.26408	-111.882705
	B	75.38	0.19	231.02	1.42	63.00	0.12	2400.16	10.72	4.163	0.022	0.582	-3.95		
	C	14.00	0.05	163.04	1.09	49.40	0.14	563.97	3.61	2.907	0.022	0.584	-25.6		
	D	14.02	0.04	184.47	1.75	58.30	0.30	478.49	5.14	2.475	0.038	0.647	-4.09		
	E	11.04	0.03	186.67	1.46	58.50	0.20	375.68	3.03	2.568	0.028	0.675	-3.46		
A1408 Tanner member	F	7.58	0.02	18.43	0.24	3.32	0.05	4546.46	71.10	10.056	0.161	0.951	770 Ma	36.10946	-111.845596
	G	4.39	0.01	25.73	0.30	4.58	0.06	1904.04	23.21	10.228	0.132	0.890	-48.64		
	H	24.26	0.06	26.40	0.31	5.09	0.06	9484.14	104.06	10.126	0.117	0.900	-14.35		
													-112.3		

^aRho is the associated error correlation (Ludwig, 1980).

^bOsi is calculated at 757, 740 and 770 Ma, respectively

Uncertainties are given as 2σ for ¹⁸⁷Re/¹⁸⁸Os and ¹⁸⁷Os/¹⁸⁸Os and ¹⁸²Os.

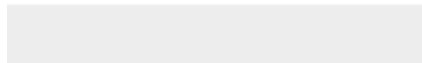
The uncertainty includes the 2 SE uncertainty for mass spectrometer analysis plus uncertainties for Os blank abundance and isotopic composition.

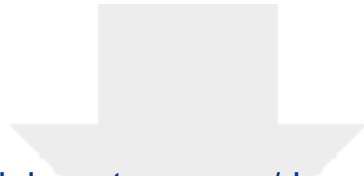


[Click here to access/download](#)

Supplemental file

Rooney-et al-GSAB-Supp-Table-1.xlsx





[Click here to access/download](#)

Supplemental file

Rooney-et al-GSAB-Supp-Table-2.xlsx

